Acta Pharmaceutica Sinica B 2026;16(7):4634−4653

Chinese Pharmaceutical Association
Institute of Materia Medica, Chinese Academy of Medical Sciences

Acta Pharmaceutica Sinica B

www.elsevier.com/locate/apsb
www.sciencedirect.com

ORIGINAL ARTICLE

Harnessing the spleen−brain axis: Magnolol-loaded nanomedicine attenuates ischemic stroke *via* oxidative stress mitigation and monocyte/macrophage reprogramming

Yane Li[a,†], Li Yao[b,†], Jiaxuan Hou[a], Xingyun Yuan[c], Yuanyuan Zhu[d], Zhichao Deng[d], Chenxi Xu[d], Jinxing Chen[a], Bingyi Chen[a], Jiayan Li[a], Yifan Mei[a], Shuang Liu[a], Shaoying Lu[a,*], Mingzhen Zhang[d,*], Hui Cai[a,*]

[a]*Department of Vascular Surgery, The First Affiliated Hospital of Xi'an Jiaotong University, Xi'an 710061, China*
[b]*Department of Neurology, XD Group Hospital, Xi'an 710077, China*
[c]*Department of Neurology, The First People's Hospital of Xianyang, Xianyang 712000, China*
[d]*School of Basic Medical Sciences, Xi'an Jiaotong University, Xi'an 710061, China*

Received 6 September 2025; received in revised form 14 January 2026; accepted 8 February 2026

KEY WORDS

Spleen−brain axis;
Ischemic stroke;
Cerebral ischemia−reperfusion injury;
Magnolol;
Liposomes;
Splenic monocytes/macrophages;
Oxidative stress;
Macrophage polarization

Abstract Cerebral ischemia−reperfusion (I/R) injury is exacerbated by the infiltration of splenic monocytes/macrophages (Mo/Mϕ) *via* the spleen−brain axis, where splenic-derived Mo/Mϕ migrate to cerebral lesions through C−C chemokine ligand 2/receptor 2 (CCL2/CCR2) chemotaxis, thereby amplifying oxidative stress and the neuroinflammatory cascade. Building on this endogenous pathway, we devised a delivery strategy that utilizes splenic Mo/Mϕ as "living vehicles" for targeted drug delivery. To this end, we developed a spleen-targeted magnolol liposome (Mag-PEG$_{5K}$) through optimized PEGylation, ensuring its spleen-specific accumulation and uptake by splenic Mo/Mϕ. After cerebral I/R injury, these nanoparticle-laden cells migrate to the ischemic brain *via* the CCR2/CCL2 axis to remodel the immunomodulatory microenvironment. This targeted system orchestrates dual therapeutic mechanisms within the lesion: mitochondria-directed reactive oxygen species (ROS) scavenging mitigates oxidative stress and peroxisome proliferator-activated receptor gamma (PPARγ) activation reprograms macrophage polarization, suppressing pro-inflammatory M1 differentiation and curtailing tumor necrosis factor-alpha

*Corresponding authors.
E-mail addresses: robertlu@mail.xjtu.edu.cn (Shaoying Lu), mzhang21@xjtu.edu.cn (Mingzhen Zhang), caihui@xjtufh.edu.cn (Hui Cai).
[†]The authors made equal contributions to this work.
Peer review under the responsibility of Chinese Pharmaceutical Association and Institute of Materia Medica, Chinese Academy of Medical Sciences.

https://doi.org/10.1016/j.apsb.2026.02.012

(TNF-α) and interleukin-1beta (IL-1β) secretion. The attenuated cytokine release suppresses neuronal inflammatory cascades, thereby reducing apoptosis. *In vivo*, Mag-PEG$_{5K}$ showed superior efficacy to free magnolol, effectively reducing infarct volume and improving long-term neurological outcomes. Supported by favorable biosafety, this work proposes spleen-targeted nanotherapy as an innovative strategy for reprogramming peripheral immunity *via* the spleen−brain axis, highlighting the translational potential of Mag-PEG$_{5K}$ for addressing neuroinflammation and oxidative damage in ischemic stroke.

1. Introduction

Ischemic stroke represents a global health crisis with high mortality and disability rates, and has been identified as the second most common contributor to the global burden of disease[1]. Rapid restoration of blood flow during the acute phase, achieved through thrombolysis or endovascular intervention, is critical for rescuing neurons within the ischemic penumbra[2]. However, the reperfusion process itself can trigger cerebral ischemia−reperfusion (I/R) injury, exacerbating secondary neuronal damage[3]. This phenomenon, known as the "reperfusion paradox", poses a significant clinical challenge that limits therapeutic efficacy[4]. Following cerebral I/R injury, peripheral monocytes/macrophages (Mo/Mϕ) infiltrate the ischemic brain parenchyma[5]. Within the hostile microenvironment, these infiltrating cells polarize towards a pro-inflammatory M1 phenotype, releasing substantial amounts of inflammatory cytokines, for instance, tumor necrosis factor-alpha (TNF-α) and interleukin-1beta (IL-1β)[6]. This drives a cascade of local oxidative stress and neuroinflammation, ultimately leading to neuronal apoptosis and neurological dysfunction[7]. This pathological cascade suggests that targeted modulation of peripheral Mo/Mϕ and the immune microenvironment they orchestrate may represent an efficacious therapeutic regimen against cerebral I/R injury.

The spleen serves as a crucial bridge connecting the central nervous system and the peripheral immune system following a stroke, with communication mediated through the spleen−brain axis[8]. Cerebral I/R injury triggers splenic contraction, releasing Mo/Mϕ from its reservoir[9]. These splenic-derived Mo/Mϕ migrate to the ischemic penumbra primarily *via* the C−C chemokine ligand 2/receptor 2 (CCL2/CCR2) chemotactic axis, constituting a major source of infiltrating Mo/Mϕ within the brain[10]. However, conventional strategies targeting splenic Mo/Mϕ exhibit significant limitations[11]. Splenectomy, while eliminating splenic Mo/Mϕ and reducing their accumulation in the brain, fails to confer effective neuroprotection due to its severe disruption of systemic immune homeostasis[12]. Similarly, although depletion of splenic macrophages using clodronate liposomes offers some benefits for post-ischemic tissue repair and remodeling, the newly recruited macrophages following depletion exhibit a propensity towards a pro-inflammatory phenotype, potentially hindering the recovery process[13]. Consequently, effective treatment of cerebral I/R injury requires moving beyond simple ablation of splenic Mo/Mϕ towards the development of targeted strategies that can precisely reprogram their polarization phenotype.

Magnolol, the primary bioactive constituent of the traditional Chinese herb *Magnolia officinalis*, is an ideal candidate for treating I/R injury due to its dual neuroprotective mechanisms involving potent antioxidative and anti-inflammatory effects[14]. Identified as a peroxisome proliferator-activated receptor gamma (PPARγ) agonist, magnolol has been shown to inhibit lipopolysaccharide (LPS)-induced M1 polarization of RAW264.7 macrophages *in vitro*[15]. Nevertheless, its modulatory effects on splenic Mo/Mϕ within the cerebral I/R injury microenvironment remain largely unexplored[16]. Moreover, magnolol faces significant pharmaceutical limitations, including poor aqueous solubility and limited stability, which result in insufficient accumulation at the ischemic lesion site when administered intravenously as a free drug[17]. Existing magnolol delivery systems (*e.g.*, polymeric nanoparticles, lipid nanocapsules) primarily focus on crossing the blood−brain barrier (BBB) for direct brain delivery[18]. Research leveraging the spleen−brain axis through spleen-targeted nanomedicine to modulate peripheral Mo/Mϕ polarization against cerebral I/R injury is scarce, thereby overlooking the strategic potential of this targeted immunomodulatory approach.

Herein, we propose an innovative drug delivery strategy targeting the spleen−brain axis. By optimizing PEGylation, we engineered magnolol-loaded liposomes (Mag-PEG$_{5K}$). This system achieved highly efficient and specific accumulation of magnolol in the spleen. Following cerebral I/R injury, Mag-PEG$_{5K}$ was internalized by splenic Mo/Mϕ. Subsequently, these drug-laden Mo/Mϕ functioned as "living vehicles", autonomously migrating to the ischemic penumbra guided by the CCL2/CCR2 axis. At the lesion site, Mag-PEG$_{5K}$ exerted dual pharmacological actions: mitochondria-directed reactive oxygen species (ROS) scavenging to mitigate oxidative stress, and PPARγ activation to reprogram macrophage polarization, suppressing the M1 polarization of splenic-derived Mo/Mϕ within the ischemic microenvironment, which led to a reduction in TNF-α and IL-1β secretion. Consequently, this immunomodulation attenuated hyperactivation of neuronal inflammatory cascades (including NF-κB, MAPK, and PI3K−Akt pathways), diminished neuronal apoptosis, and significantly promoted both histopathological recovery and neurological function in mice subjected to cerebral I/R injury (Fig. 1). Herein, we propose a novel immune cell vehiculization strategy that integrates spleen-targeted nanotechnology with living cell-based delivery systems, thereby addressing the inherent drawbacks of conventional strategies focused solely on BBB penetration. Our research demonstrates that spleen-targeted nanotherapy represents an effective approach for modulating peripheral immunity *via* the spleen−brain axis. This positions Mag-PEG$_{5K}$ as a promising translational nanomedicine, characterized by precise targeting, favorable biocompatibility, and therapeutic efficacy in treating stroke-related pathologies.

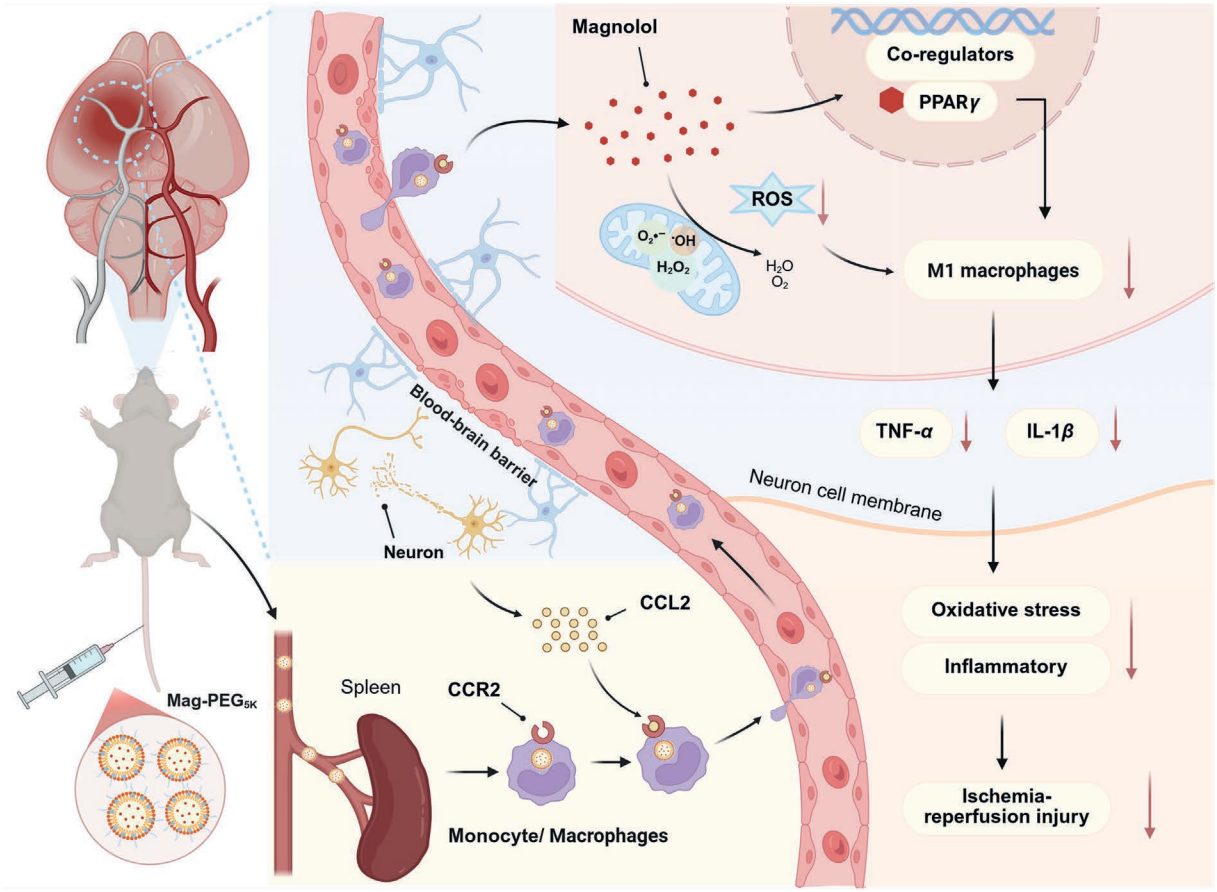

Figure 1 Schematic illustration of spleen-targeted Mag-PEG_{5K} liposomes treating cerebral ischemia−reperfusion (I/R) injury. Spleen-targeted Mag-PEG_{5K} liposomes are injected into mice *via* the tail vein and internalized by splenic monocytes/macrophages (Mo/Mϕ), which act as living vehicles and migrate to ischemic brain lesions *via* the C−C chemokine ligand 2/receptor 2(CCL2/CCR2)chemotactic axis; within the neural microenvironment, Mag-PEG_{5K} mediates reactive oxygen species (ROS) scavenging and peroxisome proliferator-activated receptor gamma (PPARγ) activation to reprogram splenic Mo/Mϕ polarization, suppress the secretion of tumor necrosis factor-alpha (TNF-α) and interleukin-1beta (L-1β), and attenuate neuronal inflammatory cascades and oxidative stress.

2. Materials and methods

2.1. *Ethics statement*

Male C57BL/6 mice, aged 8−10 weeks, were purchased from the Medical Experimental Animal Center of Xi'an Jiaotong University (Xi'an, China). All mice were maintained under constant humidity and temperature in the Medical Experimental Animal Center of Xi'an Jiaotong University (Xi'an, China) with access to food and water ad libitum. All procedures involving animals were performed following protocols approved by the Animal Ethics Committee of Xi'an Jiaotong University and conformed to the Guidelines for the Care and Use of Laboratory Animals (Approval No. XJTUAE2024-1005).

2.2. *Preparation of magnolol liposomes*

Magnolol liposomes were prepared *via* thin-film hydration coupled with membrane extrusion. Briefly, magnolol (Aladdin Biochemical Technology, Shanghai, China), Hydrogenated Soy Phosphatidylcholine (HSPC), cholesterol, and 1,2-distearoyl-*sn*-glycero-3-phosphoethanolamine-poly ethylene glycol) (DSPE-PEG) derivatives (PEG_{1K}, PEG_{2K}, PEG_{5K}, or PEG_{10K}) (Ruixi Biological Technology, Xi'an, China) were dissolved in chloroform. The organic phase was evaporated under vacuum using rotary evaporation (40 °C, 10 min) to generate thin lipid films. Films were rehydrated with phosphate-buffered saline (PBS) at 60 °C with vortex mixing at 1200 rpm for 3 min (LP Vortex Mixer, Thermo Fisher Scientific, MA, USA), then extruded through polycarbonate membranes with a pore size of 200 nm (11 cycles, 70 °C). Final formulations were stored at 4 °C. The molar ratio used for liposome preparation was HSPC: cholesterol: DSPE-PEG: magnolol = 2:1:0.19:0.1.

Magnolol, HSPC, cholesterol, and DSPE-PEG derivatives were separately mixed with 1,1′-dioctadecyl-3,3,3′,3′-tetramethylindotricarbocyanine iodide (DiR), 3,3′-dioctadecyloxacarbocyanine perchlorate (DiO), and 1,1′-dioctadecyl-3,3,3′,3′-tetramethylindocarbocyanine perchlorate (DiL) (Beyotime Biotechnology, Shanghai, China) in chloroform. The mixtures were then used to prepare DiR, DiO and DiL labeled Mag-PEG_{1K}, Mag-PEG_{2K}, Mag-PEG_{5K}, and Mag-PEG_{10K} liposomes *via* thin-film hydration coupled with membrane extrusion.

2.3. *Characterization of magnolol liposomes*

The liposomal particle size and zeta potential were measured by Malvern Zetasizer Nano ZS90 (Malvern Panalytical, Worcestershire, UK). The morphology was captured using a FEI Tecnai G2

F30 microscope (FEI Company, OR, USA). The concentration of magnolol in the samples was quantified at 293 nm using a high-performance liquid chromatography (HPLC) system (Classical 3100, Elite, Dalian, China) equipped with a SinoChrom ODS-BP C18 column (4.6 mm × 250 mm, 5 μm).

2.4. Cells

Isolation of splenic monocyte/macrophage (Mo/Mϕ): mouse spleens were harvested aseptically and placed in ice-cold Dulbecco's modified Eagle's medium (DMEM, Beyotime Biotechnology, Shanghai, China). Tissues were homogenized, filtered through a 70-μm nylon mesh, and treated with lysis buffer to remove erythrocytes. For seeding onto poly-L-lysine-coated 6-well plates, cells were first resuspended in a complete medium formulation of DMEM with 10% fetal bovine serum (FBS) and 1% penicillin/streptomycin, following three PBS washes. After 72 h of culture, adherent and non-adherent cells were removed, and adhering splenic Mo/Mϕ cells were obtained.

Isolation of brain-invading inflammatory cells: following intracardiac perfusion with ice-cold PBS, the ipsilateral ischemic hemisphere was mechanically dissociated in Roswell Park Memorial Institute (RPMI)-1640 (Beyotime Biotechnology). Tissue digestates were incubated with papain, deoxyribonuclease I (MedChemExpress, Shanghai, China), and dispase (Sigma−Aldrich, MO, USA). Inflammatory cells were isolated by 37%−70% Percoll (Solarbio, Beijing, China) density gradient centrifugation. Cells were stained with Live/Dead marker, Ly6G, CD45, CD11b, CD11c, and CD86 (BD Pharmingen, CA, USA). Flow cytometric analysis was performed to identify $DiO^+CD45^+CD11b^+CD11c^-$ cells, representing brain-infiltrating, nanomaterial-associated Mo/Mϕ.

The murine macrophage cell line RAW 264.7 (CL-0190, Procell Life Science, Wuhan, China) and mouse hippocampal neuronal cell line HT22 (CL-0697, Procell Life Science, Wuhan, China) were maintained in DMEM-based medium. This medium was supplemented with 10% FBS and 1% penicillin−streptomycin at 37 °C in a humidified 5% CO_2 incubator.

2.5. Cellular uptake

RAW264.7 cells or splenic Mo/Mϕ were co-cultured with Mag-PEG_{5K} in complete medium for 6 h. After washing with PBS, cells were stained with fluorescein isothiocyanate (FITC) or Mito-Tracker Green (Beyotime Biotechnology) for 30 min in the dark, washed, and fixed with 4% paraformaldehyde (PFA). Nuclei were counterstained with 4′,6-diamidino-2-phenylindole (DAPI) (Beyotime Biotechnology). Co-localization of the materials with FITC or Mito-Tracker Green was visualized using a Zeiss upright fluorescence microscope (Carl Zeiss, Jena, Germany).

2.6. Intracellular ROS scavenging ability

To evaluate ROS clearance, RAW 264.7 cells or splenic Mo/Mϕ were pretreated with magnolol and Mag-PEG_{5K} for 6 h, then exposed to 200 μmol/L hydrogen peroxide (H_2O_2) for 24 h. Cells were then incubated with the fluorescent ROS probes 2′,7′-dichlorofluorescin diacetate (DCFH-DA) or dihydroethidium (DHE) (Beyotime Biotechnology) for 30 min at 37 °C in the dark. Fluorescence microscopy and flow cytometry were employed to quantify intracellular ROS levels.

2.7. Polarization of splenic Mo/Mϕ and RAW264.7

Splenic Mo/Mϕ or RAW 264.7 cells were polarized to the M1 phenotype using DMEM containing 10 ng/mL Lipopolysaccharide (LPS, Sigma) for 6 h. Subsequently, cells were then co-cultured with magnolol or Mag-PEG_{5K} for 24 h. Polarization markers were quantitatively analyzed using the following three techniques: quantitative real-time polymerase chain reaction (qPCR) was employed to detect gene expression at the transcriptional level; Western blot (WB) was used to analyze specific protein expression levels; and flow cytometry was applied for the quantitative detection of cell surface markers. Primer sequences are listed in Supporting Information Table S1, and antibody details are provided in Supporting Information Table S2.

2.8. In vivo biodistribution imaging

Anesthetized C57BL/6J mice received tail vein injections of 100 μL DiR-labeled PEG_{1K}, PEG_{2K}, PEG_{5K}, or PEG_{10K} liposomes. At 2, 6, 12, 24, and 48 h after injection, whole-body near-infrared imaging was carried out. After the animals were euthanized, *ex vivo* imaging was performed to examine fluorescence in the heart, liver, spleen, lungs, kidneys, and brain.

2.9. In vivo splenic Mo/Mϕ uptake

C57BL/6J mice received 100 μL of DiL-labeled PEG_{1K}, PEG_{2K}, PEG_{5K}, or PEG_{10K} liposomes *via* the tail vein. After 12 h, spleens were harvested post cervical dislocation, dissociated through a 70-μm strainer, and treated with ACK lysis buffer. Cells were stained with: Ly6G, CD45, F4/80, CD86, and CD11b (BD Pharmingen). The percentage of $DiL^+CD45^+CD11b^+F4/80^+$ cells, representing splenic Mo/Mϕ that had internalized the nanomaterials, was determined by flow cytometry.

2.10. Transient middle cerebral artery occlusion (tMCAO) model in mice

The tMCAO model of middle cerebral artery ischemia was established in mice for a duration of 60 min, following the methods previously outlined. In summary, male C57BL/6J mice were sedated using 2% isoflurane in oxygen. Surgical exposure of the common, external, and internal carotid arteries was achieved *via* a midline neck incision. After external carotid artery ligation, middle cerebral artery occlusion was induced by the insertion of a nylon monofilament embolus. This was introduced into the ECA and advanced through the common carotid artery bifurcation into the intracranial internal carotid artery until it was positioned 10 ± 1 mm from the bifurcation, where it remained for 60 min to block cerebral blood flow. Subsequently, the nylon monofilament was removed to facilitate reperfusion. Sham-operated animals underwent an identical surgical procedure, except that the nylon monofilament was not inserted.

2.11. Enzyme-linked immunosorbent (ELISA) assay

TNF-α ELISA kits (SYP-MOO36, Upingbio Biotechnology, Shanghai, China) and IL-1β ELISA kits (SYP-MOO26, Upingbio Biology) were used to assess the levels of the cytokines TNF-α and IL-1β.

2.12. Brain immunofluorescence staining

C57BL/6J mouse brains were fixed in 4% PFA, cryoprotected by immersion in 30% sucrose. After adequate saturation, the brains were embedded in optimal cutting temperature (OCT) compound and obtained coronal sections (10 μm). After permeabilization with 0.3% Triton X-100 and blocking with 5% bovine serum albumin (BSA), sections were incubated overnight at 4 °C with primary antibodies against CCR2 (Proteintech, Wuhan, China) and ionized calcium-binding adapter molecule 1 (Iba1, Proteintech). Apoptotic cells were detected using a terminal deoxynucleotidyl transferase dUTP nick end labeling (TUNEL) assay kit (Proteintech). Sections were then incubated with appropriate Alexa Fluor-conjugated secondary antibodies (Proteintech). After counterstaining with DAPI, slides were imaged using a fluorescence microscope.

2.13. 2,3,5-Triphenyltetrazolium Chloride (TTC) staining

For the assessment of cerebral infarction, brains were rapidly extracted and frozen (−20 °C, 20 min). Coronal slices (2 mm thick) were prepared and incubated in a 2% TTC (Sigma) for 30 min at 37 °C in the dark and then fixed in 4% PFA.

2.14. Hematoxylin and eosin (H&E) and Nissl staining

Brain tissues were processed for paraffin embedding and sectioned. One set of sections was stained with H&E for general morphology. An adjacent set was stained with Nissl solution (Beyotime Biotechnology) to assess neuronal injury and survival under a light microscope.

2.15. Neurological function test

Neurological assessments were performed by researchers blinded to the experimental groups. (1) Modified Neurological Severity Score (mNSS): At scheduled intervals (1, 3, 7, 14, 21, and 28 days) after the tMCAO procedure, blinded researchers evaluated neurological deficits based on motor, sensory, reflex, and balance tests. Scores ranged from 0 to 18, with higher scores indicating more severe impairment. The final score for each mouse was the average of the scores assigned by the blinded researchers. (2) Cylinder Test: Mice were placed in a transparent cylinder (10 cm diameter, 15 cm height), and the number of independent contacts made by each forelimb against the cylinder wall during a 5-min exploratory period was recorded. (3) Adhesive Test: A small adhesive patch (3×3 mm^2) was placed on the ventral surface of each forepaw. The time taken for the mouse to sense and remove each patch was recorded. (4) The Morris Water Maze test: Spatial learning and memory were assessed from Days 22 to 28 post-tMCAO. Mice were trained to find a hidden platform submerged in a pool of opaque water using spatial cues. Escape latency and path length were recorded. During the probe trial on Day 28, the platform was removed, and the time spent in the target quadrant and the number of platform crossings were recorded automatically by video tracking software.

2.16. Statistical analysis

Statistical analysis was conducted using GraphPad Prism 10. Data are expressed as mean ± SD from at least three independent experiments. Differences between two groups were assessed by Student's *t*-test, while multiple groups were compared using one-way ANOVA with Tukey's test. Significance levels are indicated as follows: ns (not significant), $*P < 0.05$, $**P < 0.01$, $***P < 0.001$.

3. Results and discussion

3.1. Splenic Mo/Mϕ migrate to the ischemic brain via the CCR2/CCL2 axis

The spleen serves as a critical reservoir for peripheral immune cells and is a primary source of circulating Mo/Mϕ[19]. To investigate the role of splenic Mo/Mϕ and their migration in cerebral I/R injury, we analyzed their infiltration dynamics into the ischemic brain and characterized the expression profile of the CCL2/CCR2 chemokine axis. Flow cytometry quantification revealed a significant increase in $Ly6G^-CD45^+CD11b^+CD11c^-$ Mo/Mϕ infiltration into ischemic brain tissue 24 h post-I/R compared to the sham group (Fig. 2A and B). However, splenectomy markedly attenuated this cerebral infiltration, confirming the spleen as a major source of brain-infiltrating Mo/Mϕ during the early I/R injury[20].

To elucidate the recruitment mechanism, we examined the expression of the key chemokine axis CCL2/CCR2. Immunofluorescence staining of brain cryosections demonstrated a substantial accumulation of $CCR2^+$ cells within the ischemic core (Fig. 2C and D). Furthermore, significant upregulation of both *Ccr2* (Fig. 2F) and *Ccl2* (Fig. 2E) mRNA expression was detected within the affected tissue. Notably, brain infiltration by splenic Mo/Mϕ was significantly reduced under *Ccr2* gene deficiency or following CCR2 blockade with a specific antagonist antibody[21]. This indicates that CCR2 signaling is a critical step for the egress of splenic Mo/Mϕ into the circulation[22,23]. *In vitro* Transwell migration assays further demonstrated that homogenates from I/R-injured brain tissue induced splenic Mo/Mϕ migration. Crucially, pretreatment with the CCR2-specific antagonist RS504393 significantly inhibited this migration (Fig. 2G−I). RS504393 antagonizes CCR2 specifically without detectable off-target effects (Supporting Information Fig. S1). These results collectively demonstrate that the CCL2/CCR2 axis plays a central role in mediating the migration of splenic Mo/Mϕ to the ischemic brain.

Based on these findings, we propose a spleen-targeted nanoparticle delivery strategy leveraging the spleen−brain axis. Our data collectively demonstrate the spleen as a critical reservoir and the CCR2/CCL2 axis as a key mediator within this pathway during cerebral I/R injury. Given the high CCR2 expression on splenic Mo/Mϕ, these cells can serve as "living vehicles". Drug-loaded nanoparticles are internalized by splenic Mo/Mϕ *in vivo*. Subsequently, *via* the CCL2/CCR2 axis, these nanoparticle-laden Mo/Mϕ egress from the spleen, infiltrate the ischemic brain region, and achieve targeted drug delivery to the lesion site. This strategy not only exploits the natural migratory pathways of the spleen−brain axis but also aims to remodel the post-ischemic immune microenvironment, thereby alleviating I/R injury.

3.2. Preparation and characterization of spleen-targeted magnolol liposomes

Magnolol, the primary active component of the traditional Chinese herb *Magnolia officinalis*[24], exhibits antioxidant and anti-inflammatory activities, demonstrating therapeutic potential for

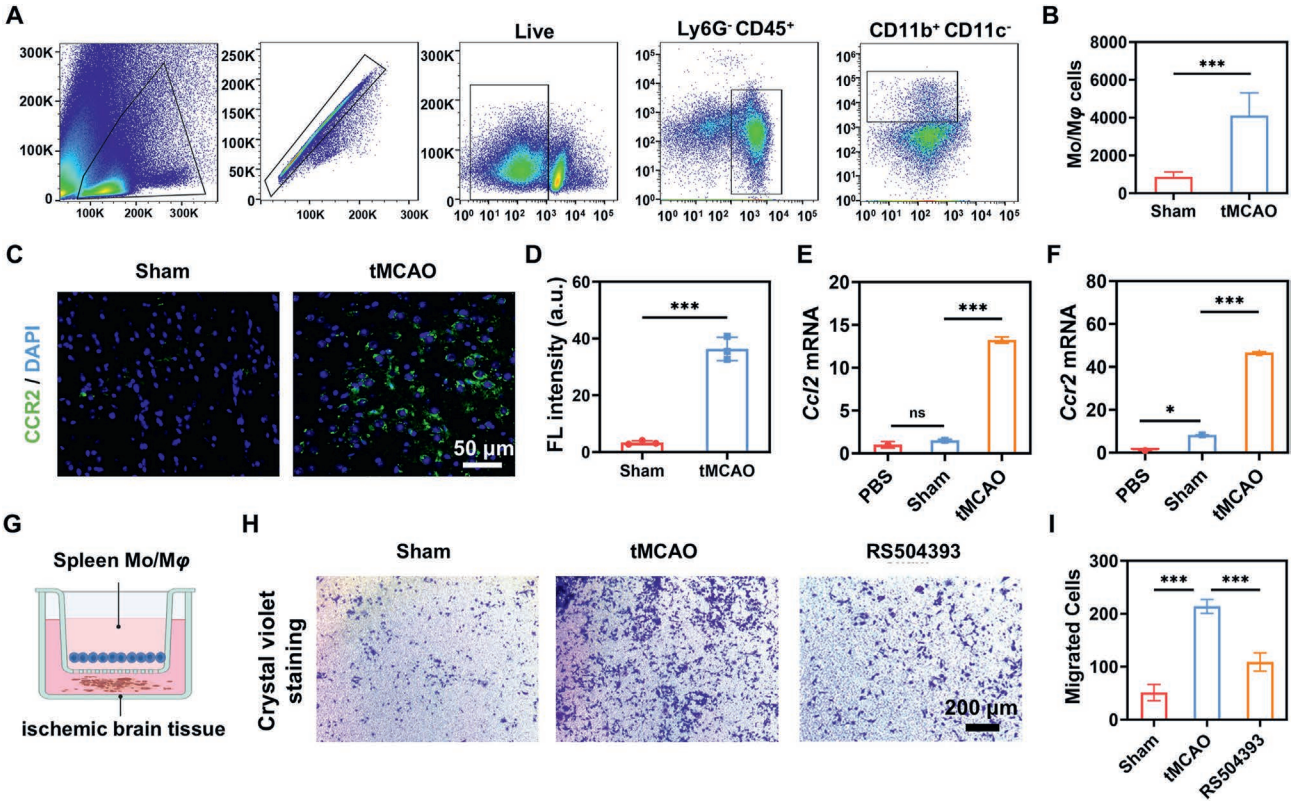

Figure 2 Splenic Mo/Mϕ migrate to the ischemic brain *via* the CCR2/CCL2 axis. Mice 24 h after cerebral I/R injury: Flow cytometry analysis (A) and quantification (B) of Ly6G$^-$CD45$^+$CD11b$^+$CD11c$^-$ Mo/Mϕ in the ischemic brain tissue ($n = 3$). (C, D) Immunofluorescence staining of CCR2$^+$ splenic Mo/Mϕ (green) in the ischemic brain region. mRNA expression levels of *Ccr2* (F) and *Ccl2* (E) in ischemic brain tissue ($n = 3$). (G) Schematic diagram of the transwell migration assay. Crystal violet staining (H) and quantification (I) of splenic Mo/Mϕ that migrated toward I/R injured brain homogenate ($n = 3$). Data are presented as mean ± SD. Statistically significant difference: ns (not significant), $^*P < 0.05$, $^{**}P < 0.01$, $^{***}P < 0.001$. Unpaired *t*-test (B)−(D) and one-way ANOVA with Tukey's test (E, F) were used for statistical analysis.

cerebral ischemic diseases[25]. However, its poor aqueous solubility and chemical stability limit its application in treating cerebral I/R injury[26]. Studies indicate that encapsulating hydrophobic drugs within liposomes can overcome solubility limitations[27]. As highly versatile nanocarriers, liposomes exhibit excellent biocompatibility and high drug-loading capacity for hydrophobic compounds[28].

The unique physiological structure and immune function of the spleen play a pivotal role in the passive splenic targeting of PEGylated liposomes. The red pulp of the spleen acts as a mechanical filter for blood, efficiently trapping senescent red blood cells and foreign particles, including nanoparticles. PEGylated magnolol liposomes with sizes ranging between 150 and 250 nm are more readily accumulated in the spleen[29]. Once sequestered in the spleen, these PEGylated liposomes are recognized as "foreign substances" by Mo/Mϕ and subsequently phagocytosed. Their structural similarity to cell membranes further facilitates this active phagocytosis by Mo/Mϕ[30]. Additionally, PEGylation prolongs the circulation time of liposomes in the bloodstream, reducing their rapid clearance by the liver[31]. This extended circulation provides more opportunities for the liposomes to be filtered and accumulated by the spleen, thereby achieving passive splenic targeting of the PEGylated liposomes[32].

Building upon this foundation, we prepared magnolol-loaded liposomes using distinct PEG-DSPE block copolymers (molecular weights: 1000, 2000, 5000, and 10,000 Da), HSPC, and cholesterol (Fig. 3A). These formulations were designated Mag-PEG$_{1K}$, Mag-PEG$_{2K}$, Mag-PEG$_{5K}$, and Mag-PEG$_{10K}$, respectively. Transmission electron microscopy (TEM) images revealed that all liposomes exhibited characteristic spherical morphology (Fig. 3B−E)**.** Dynamic light scattering (DLS) analysis showed hydrodynamic diameters of 131.5 ± 2.4 nm, 141.8 ± 1.6 nm, 147.3 ± 1.5 nm, and 156.5 ± 0.9 nm for Mag-PEG$_{1K}$, Mag-PEG$_{2K}$, Mag-PEG$_{5K}$, and Mag-PEG$_{10K}$ (Fig. 3F). Corresponding PDI values were 0.12 ± 0.02, 0.15 ± 0.01, 0.08 ± 0.02, and 0.16 ± 0.02, respectively. All values were below 0.2, indicating a narrow size distribution (Supporting Information Fig. S2). Corresponding zeta potentials were −16.6 ± 1.1 mV, −22.5 ± 0.3 mV, −27.6 ± 0.9 mV, and −25.5 ± 0.2 mV, respectively (Fig. 3G).

Stability assessment demonstrated that after 14 days in pH 7.4 PBS, the increase in particle size was 10.33%, 3.34%, 4.13%, and 3.78%, respectively (Fig. 3H). Following 4-day incubation in 10% FBS, size changes increased to 28.6%, 13.9%, 11.4%, and 12.8%, respectively (Fig. 3I). According to established nanocarrier stability criteria (particle size change <20% indicates stability), Mag-PEG$_{2K}$, Mag-PEG$_{5K}$, and Mag-PEG$_{10K}$ exhibited excellent stability.

HPLC analysis demonstrated encapsulation efficiencies of 78.2%, 85.1%, 91.9%, and 75.2%, corresponding to drug loading contents of 22.4%, 20.1%, 12.7%, and 6.14% for the respective formulations (Fig. 3J and K). *In vitro* release studies indicated

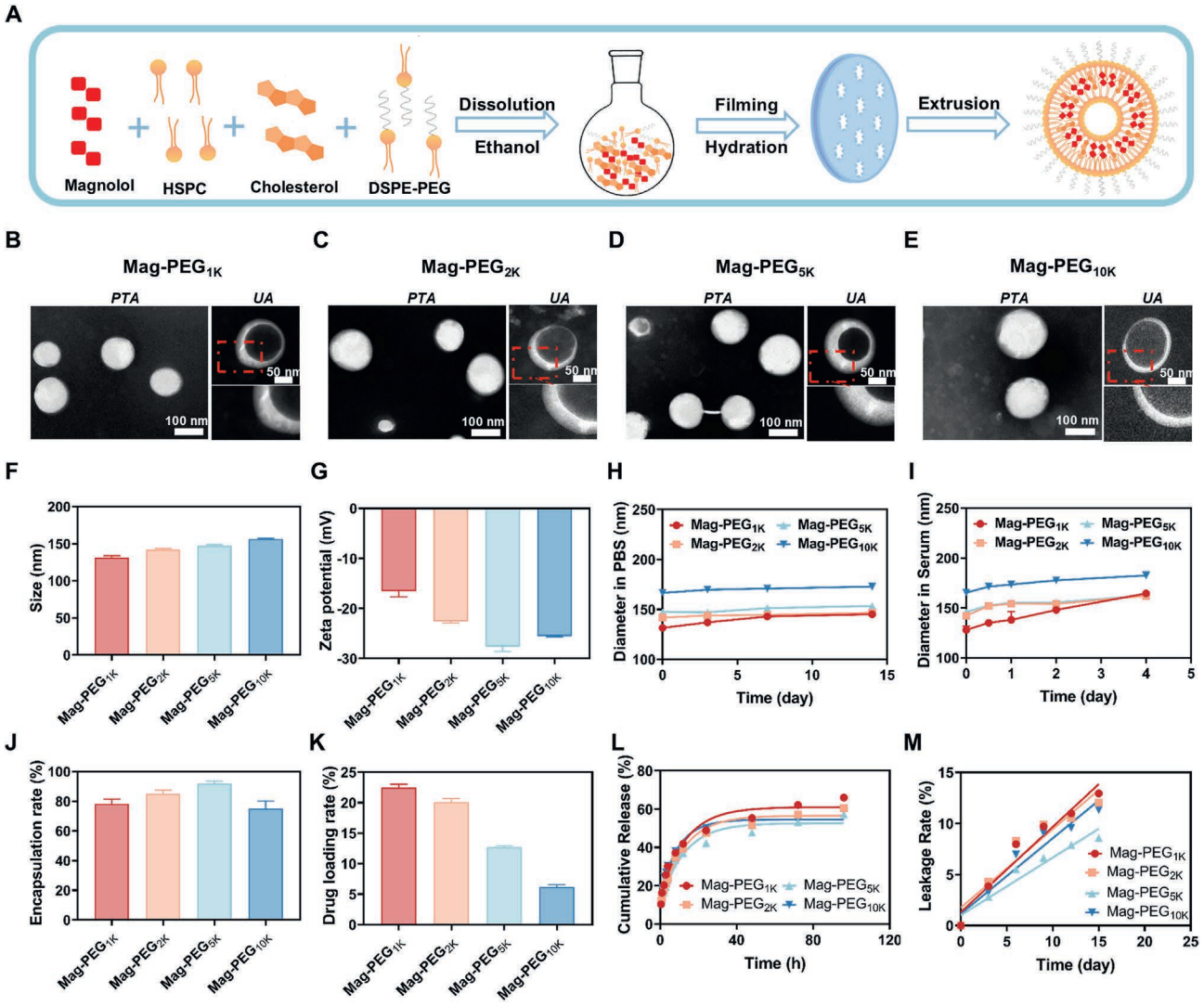

Figure 3 Preparation and characterization of spleen-targeted magnolol liposomes. (A) The preparation of magnolol liposomes. Transmission electron microscopy image of (B) Mag-PEG$_{1K}$, (C) Mag-PEG$_{2K}$, (D) Mag-PEG$_{5K}$, (E) Mag-PEG$_{10K}$ with phosphotungstic acid (PTA, left) and uranyl acetate (UA, right). Scale bar:100 or 50 nm. (F) Hydrodynamic diameter and (G) zeta potential measurements of magnolol liposomes ($n = 3$). Size changes of after magnolol liposomes being incubated in (H) PBS and (I) serum for 14 days ($n = 3$). (J) Encapsulation efficiency and (K) loading efficiency of magnolol among different liposomes ($n = 3$). (L) Cumulative released amount and (M) leakage amount of magnolol from magnolol liposomes ($n = 3$). Data are presented as mean ± SD.

sustained magnolol release profiles from all liposomes over 72 h in PBS containing 10% serum at 37 °C (Fig. 3L). Storage stability tests showed drug leakage rates of 12.9%, 12.0%, 8.6%, and 11.3% after 14 days at room temperature (Fig. 3M). Taken together, Mag-PEG$_{5K}$ demonstrated superior encapsulation stability with the lowest leakage rate (<10%). In summary, we successfully developed stable magnolol-loaded liposomal systems.

3.3. Spleen accumulation and splenic Mo/Mϕ-mediated brain delivery of magnolol liposomes

Prior studies indicate that PEG$_{5K}$-modified liposomes, due to their optimal size and surface charge matching the filtration structure of the spleen, avoid capture by hepatic Kupffer cells, thereby significantly enhancing splenic accumulation and achieving efficient passive spleen targeting[33,34]. To validate the spleen-targeting capability of magnolol liposomes, DiR-labeled liposomes were injected into mice *via* the tail vein. *In vivo* fluorescence imaging and *ex vivo* organ scanning were performed at 2, 6, 12, 24, and 48 h post-injection. Live imaging and quantitative analysis revealed that signals from DiR-Mag-PEG$_{1K}$, DiR-Mag-PEG$_{2K}$, and DiR-Mag-PEG$_{10K}$ primarily accumulated in the liver, whereas DiR-Mag-PEG$_{5K}$ exhibited significantly elevated fluorescence signals in the spleen, with sustained presence for up to 48 h (Fig. 4A–F). The aggregation intensity of DiR-Mag-PEG$_{5K}$ in the spleen was markedly higher than that of liposomes modified with other PEG chain lengths (Fig. 4G). Furthermore, the quantitative targeting index, calculated as the fluorescence intensity ratio of the spleen to other major organs, consistently exceeded 1 across all time points, confirming the superior and specific accumulation of Mag-PEG$_{5K}$ in the spleen (Supporting Information Fig. S3). Consistently, HPLC analysis of tissue samples at 12 h post-injection revealed a significantly higher concentration of

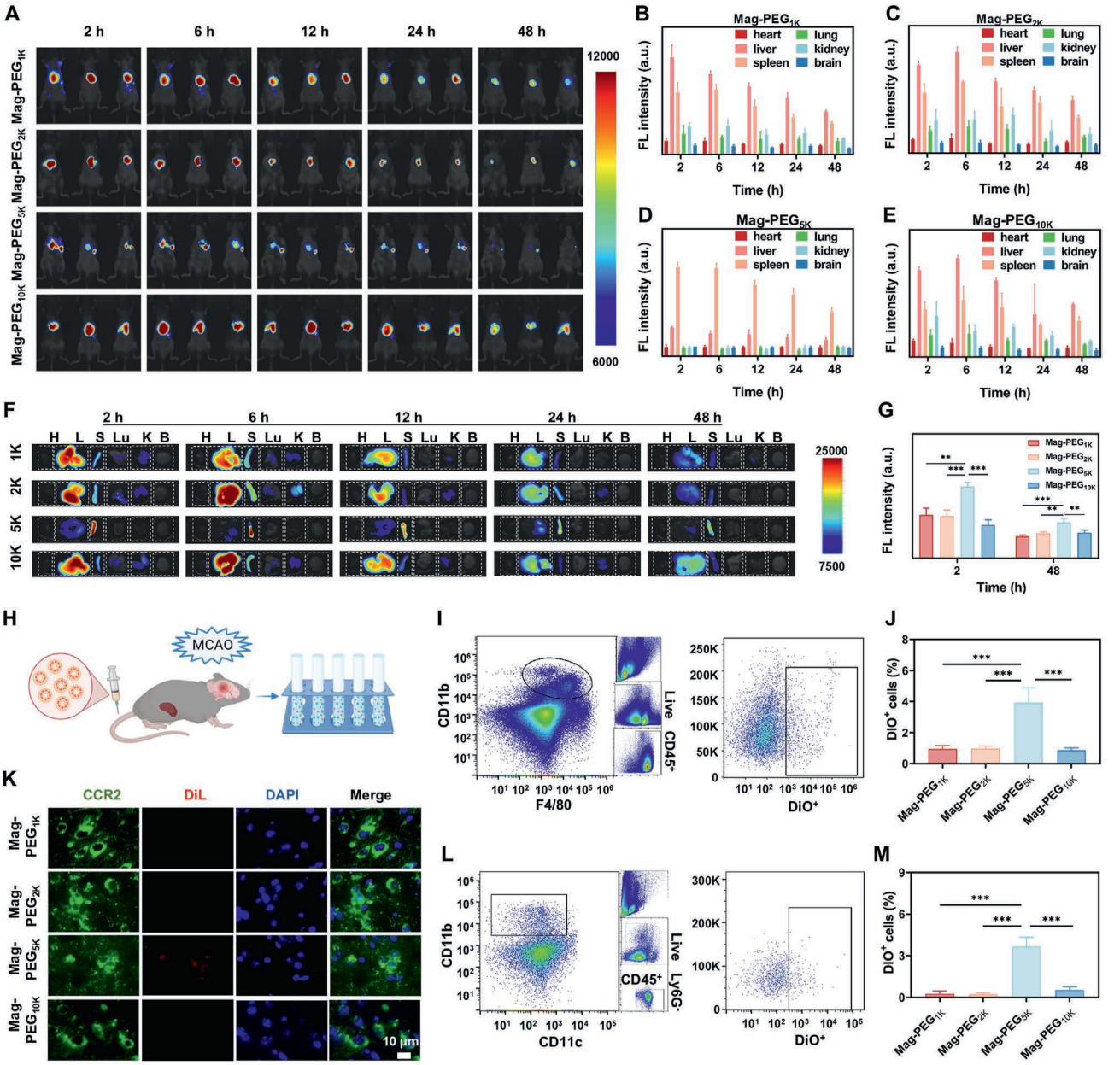

Figure 4 Spleen accumulation and splenic Mo/Mϕ-mediated brain delivery of magnolol liposomes. Fluorescence imaging of (A) normal mice and (F) organs scanning at different timepoints after tail-vein injection with DiR-labeled magnolol liposomes. Quantitative analysis of the distribution of (B) Mag-PEG$_{1K}$, (C) Mag-PEG$_{2K}$, (D) Mag-PEG$_{5K}$, and (E) Mag-PEG$_{10K}$ in *ex vivo* organs at different times ($n = 3$). (G) Quantification of mean fluorescence intensity of the spleen in different liposome groups at 2 and 48 h ($n = 3$). (H) Schematic illustration of flow cytometry in mice 24 h after cerebral I/R injury. Co-localization of splenic Mo/Mϕ and DiO-labeled magnolol liposomes in (I, J) spleen and (L, M) ischemic brain tissue ($n = 5$). (K) Co-localization images of splenic macrophages (CCR2, green) and DiL-labeled magnolol liposomes (red) in the ischemic penumbra. Scale bar: 10 μm. Data are presented as mean ± SD. Statistically significant difference: $^{**}P < 0.01$, $^{***}P < 0.001$. One-way ANOVA with Tukey's test was used for statistical analysis.

magnolol in the spleens of the Mag-PEG$_{5K}$ group compared to other formulations (Supporting Information Fig. S4). Finally, the pharmacokinetic profile demonstrated that the concentration of magnolol delivered *via* Mag-PEG$_{5K}$ liposomes in the plasma and brain was substantially greater than that of free magnolol at all measured time points (Supporting Information Fig. S5), indicating enhanced systemic circulation and more effective brain delivery.

Given the known migration of splenic Mo/Mϕ to cerebral ischemic regions *via* the CCL2/CCR2 chemotactic axis[35], we further investigated whether magnolol liposomes could be internalized by splenic Mo/Mϕ and transported to the brain. In the tMCAO mouse model, flow cytometry analysis was performed after tail vein injection of DiO-labeled liposomes (DiO-Mag-PEG$_{1K}$, DiO-Mag-PEG$_{2K}$, DiO-Mag-PEG$_{5K}$, and DiO-Mag-PEG$_{10K}$) (Fig. 4H). The results of flow cytometry demonstrated that splenic Mo/Mϕ effectively internalized DiO-Mag-PEG$_{5K}$ (Fig. 4I and J). Brain tissue flow cytometry revealed co-localization of migrated splenic-derived Mo/Mϕ with DiO-Mag-

PEG_{5K} in the brain, whereas non-spleen-targeting liposomes (DiO-Mag-PEG_{1K}, DiO-Mag-PEG_{2K}, and DiO-Mag-PEG_{10K}) showed near-zero co-localization (Fig. 4L and M). This confirmed spleen targeting is essential for this spleen−brain delivery pathway.

To exclude the possibility that liposomes directly penetrated the damaged blood−brain barrier (BBB) and were subsequently taken up by Mo/Mϕ or microglia, brain cryosections from mice injected with DiI-Mag-PEG_{5K} were co-stained with CCR2 and Iba-1 antibodies. Results showed co-localization of DiI-Mag-PEG_{5K} with $CCR2^+$ Mo/Mϕ in the ischemic area (Fig. 4K), but no co-localization with Iba-1^+ microglia (Supporting Information Fig. S6), indicating that the Mag-PEG_{5K} primarily relied on active migration of splenic Mo/Mϕ *via* the CCR2/CCL2 axis. Collectively, these results establish the feasibility of utilizing splenic Mo/Mϕ as "living vehicles" to transport therapeutic liposomes to cerebral ischemic lesions *via* the spleen−brain axis.

3.4. ROS-scavenging and macrophage reprogramming of Mag-PEG_{5K}

Previous *in vitro* experiments confirmed that Mag-PEG_{5K} possesses splenic targeting properties, can be internalized by splenic Mo/Mϕ, and subsequently delivered to the ischemic cerebral hemisphere *via* the spleen−brain axis. Based on this, we further investigated the cellular antioxidant activity of Mag-PEG_{5K} and its regulatory effect on macrophages *in vitro*.

We initially assessed the ROS-scavenging capacity of magnolol and Mag-PEG_{5K} in the culture medium. As shown in Supporting Information Fig. S7, both compounds demonstrated favorable overall antioxidant activity and could potently scavenge superoxide anion ($O_2^{\bullet-}$) and hydroxyl radicals (OH). No statistically significant difference was observed between the two groups, indicating that magnolol and Mag-PEG_{5K} possess comparable ROS-scavenging capacities in the culture medium, and the liposomal carrier did not impair the activity of magnolol.

Cellular uptake represents the initial step for Mag-PEG_{5K} to exert its biological effects. We utilized DiL-labeled Mag-PEG_{5K} (DiL-Mag-PEG_{5K}) to visualize its internalization process. Following 6 h co-incubation of DiL-Mag-PEG_{5K} with splenic Mo/Mϕ or RAW264.7 cells, it was observed that both cell types efficiently took up Mag-PEG_{5K}, with the uptake efficiency exhibiting a time-dependent pattern, reaching a level of 93.2% at 6 h (Fig. 5A and Supporting Information Fig. S8). Given that ROS is a critical factor promoting the polarization of Mo/Mϕ toward the M1 phenotype, and mitochondria are a major source of ROS following cellular injury[36,37], the subcellular localization of Mag-PEG_{5K} was further examined. Following mitochondrial labeling with Mito-Tracker, the Pearson correlation coefficient between Mag-PEG_{5K} and mitochondria in splenic Mo/Mϕ was 0.96, and that in RAW264.7 cells was 0.84 (Fig. 5B−D and Supporting Information Fig. S9). These results indicate that Mag-PEG_{5K} exhibits a significant mitochondrial targeting ability[38].

Next, we employed DCFH-DA and DHE probes to evaluate the intracellular ROS-scavenging efficacy of Mag-PEG_{5K} in splenic Mo/Mϕ. In comparison to the control group, the H_2O_2-treated group exhibited significantly enhanced intracellular fluorescence signals (Fig. 5E), confirming elevated ROS levels. In contrast, treatment with either magnolol or Mag-PEG_{5K} significantly reduced the levels of ROS. Notably, at equivalent molar concentrations of magnolol, the Mag-PEG_{5K} group exhibited superior ROS-scavenging efficacy compared to the free magnolol group, which was further quantified and validated by flow cytometry analysis (Fig. 5F and G). Considering the diversity and heterogeneity of splenic Mo/Mϕ, we replicated these experiments in the RAW264.7 cell line, yielding consistent results (Supporting Information Fig. S10). To determine whether Mag-PEG_{5K} scavenges ROS *via* mitochondrial targeting, we performed co-localization analysis using MitoSOX Red and Mito-Tracker Green. Mag-PEG_{5K} effectively localized to mitochondria and markedly reduced the MitoSOX signal (Supporting Information Fig. S11). This enhanced efficacy is attributed to the protective effect of the liposomes and the significantly improved cellular uptake efficiency, thereby facilitating the targeted delivery of the drug to mitochondrial sites with high ROS production and more effectively suppressing H_2O_2-induced intracellular ROS accumulation.

In cerebral I/R injury, as a key second messenger, ROS can synergize with inflammatory signals to promote macrophage polarization toward the M1 phenotype[39]. To investigate the role of ROS in macrophage polarization, we treated Mo/Mϕ with H_2O_2 and examined the expression levels of M1 macrophage markers CD86, TNF-α, and IL-1β. The results showed that the H_2O_2-treated group exhibited higher expression levels of CD86, TNF-α, and IL-1β compared to the control group, indicating that H_2O_2 treatment induces M1 macrophage polarization (Fig. 5H−J). In contrast, the Mag-PEG_{5K} group demonstrated significantly lower expression levels of TNF-α and IL-1β compared to both the H_2O_2 and magnolol groups, suggesting that Mag-PEG_{5K} treatment effectively suppresses M1 polarization. These data demonstrate that scavenging excess intracellular ROS helps inhibit M1 polarization in macrophages stimulated by H_2O_2.

To elucidate the regulatory mechanism, we screened magnolol's target profile and identified peroxisome proliferator-activated receptor γ (PPARγ) as the core regulatory factor (Supporting Information Fig. S12). Molecular docking (AutoDock Vina) revealed that PPARγ could bind two magnolol molecules within its ligand-binding domain with binding energies of −8.0 and −7.2 kcal/mol, confirming PPARγ as a target (Fig. 5K). PPARγ is highly expressed in macrophages, and activation of its signaling pathway can inhibit macrophage polarization toward the M1 phenotype[40]. To verify whether Mag-PEG_{5K} regulates splenic macrophage polarization by activating the PPARγ pathway in the context of cerebral I/R injury, we utilized LPS-stimulated macrophages as an *in vitro* model. Western blot analysis results showed that compared with the control group, the LPS group exhibited a significant decrease in *p*-PPARγ expression (Fig. 5L). Following intervention with magnolol or Mag-PEG_{5K}, the phosphorylation level of PPARγ in splenic macrophages was significantly elevated, with Mag-PEG_{5K} exerting a more pronounced effect. In contrast, empty liposomes (PEG_{5K}) had no significant impact on PPARγ expression (Fig. 5M). To confirm the critical role of PPARγ, we employed the PPARγ antagonist GW9662 for counter-validation. The results demonstrated that GW9662 treatment reversed the activating effect of Mag-PEG_{5K} on the PPARγ signaling pathway and its inhibitory effect on M1 macrophages, restoring the expression levels of CD86 and the pro-inflammatory cytokines TNF-α and IL-1β (Fig. 5N). Consistently, Mag-PEG_{5K} upregulated the PPARγ downstream genes *Cd36* and *Fabp4* at mRNA and protein levels, an effect blocked by GW9662 (Fig. 5O and P).

To clarify the molecular mechanism by which Mag-PEG_{5K} regulates macrophage polarization through PPARγ, we performed chromatin immunoprecipitation-quantitative polymerase chain reaction (ChIP-qPCR). PPARγ did not bind directly to promoters

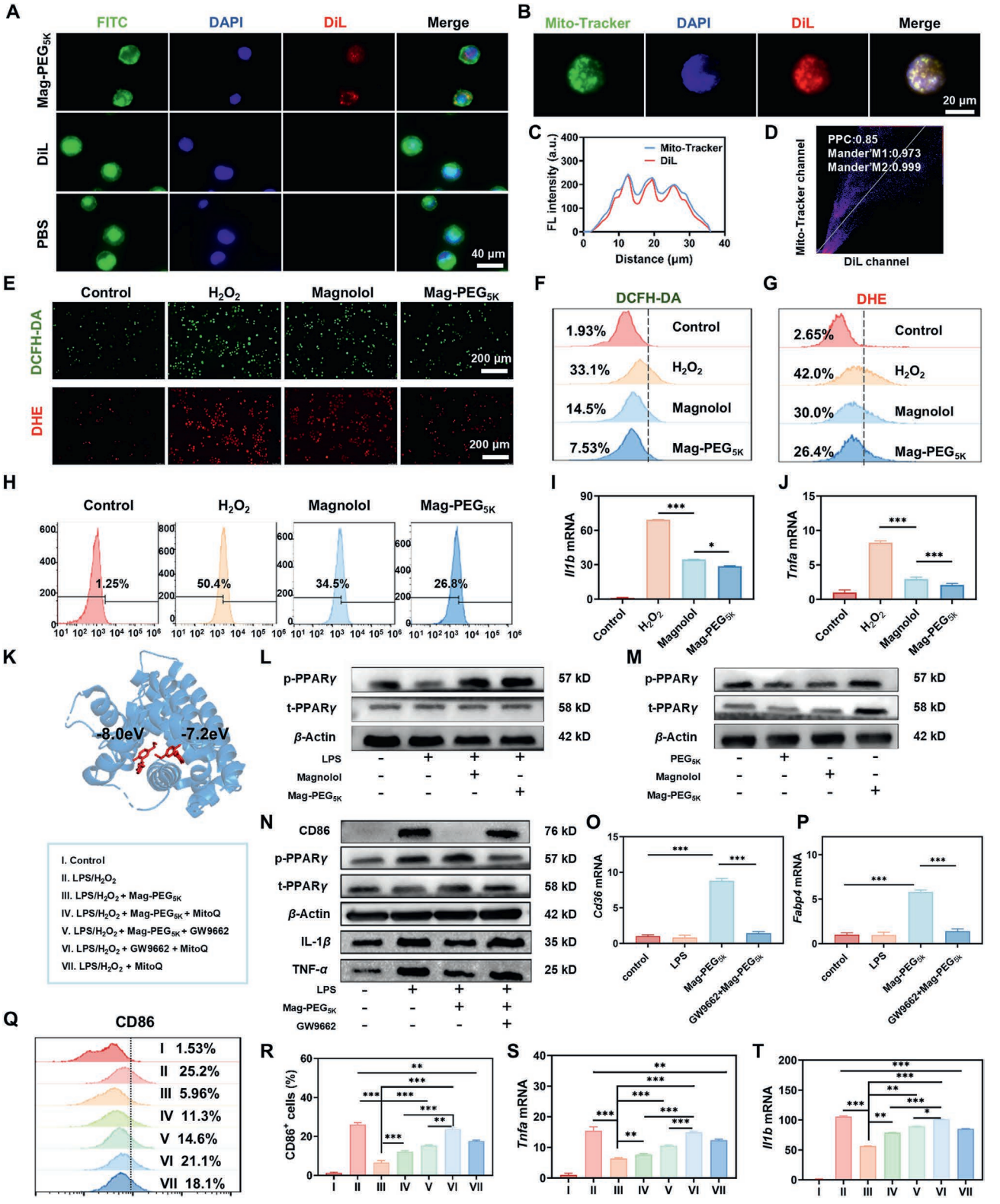

Figure 5 ROS-scavenging and macrophage reprogramming of Mag-PEG$_{5K}$. (A) Intracellular localization of DiL-Mag-PEG$_{5K}$ in Mo/Mϕ. Scale bar: 40 μm. (B) Co-localization of DiL-Mag-PEG$_{5K}$ with mitochondria. Scale bar: 20 μm. (C) Mander's correlation coefficient (MCC) analyses and (D) Pearson's correlation coefficient (PCC) of DiL-Mag-PEG$_{5K}$ with mitochondria. (E) Representative images of DCFH-DA and DHE. Scale bar: 200 μm. Flow cytometry of (F) DCFH-DA and (G) DHE in splenic Mo/Mϕ. (H) Flow cytometry analysis of CD86. Gene expression of (I) *Il1b*, and (J) *Tnfa* ($n = 3$). (K) Docking image between magnolol and PPARγ molecules. (L, M) Western blot of the protein levels of t-PPARγ and *p*-PPARγ. (N) Western blot of t-PPARγ, *p*-PPARγ, CD86, IL-1β, and TNF-α. Gene expression of (O) *Cd36*, and (P) *Fabp4* ($n = 3$). (Q, R) Flow cytometry analysis of CD86. Gene expression of (T) *Il1b* and (S) *Tnfa* ($n = 3$). Data are presented as mean ± SD. Statistically significant difference: $^{*}P < 0.05$, $^{**}P < 0.01$, $^{***}P < 0.001$. One-way ANOVA with Tukey's test was used for statistical analysis.

of M1 genes (*Cd86*, *Tnf*) or the M2 gene *Cd206*, but showed specific binding to the promoter of the M2 gene *Arg1* (Supporting Information Fig. S13). Consistent with previous literature reports[8,41-43], PPARγ can indirectly regulate M1 gene transcription *via* NF-κB and directly activate Arg1 transcription, shifting the balance toward an M2 phenotype.

To elucidate the mechanistic relationship between ROS scavenging and PPARγ activation in Mag-PEG_{5K}-mediated regulation of macrophage polarization under cerebral I/R injury-like conditions, we established an *in vitro* inflammatory and oxidative stress model using LPS/H_2O_2 co-stimulation of splenic macrophages. Seven experimental groups (I−VII) were analyzed for M1 polarization markers *Cd86*, *Tnfa*, and *Il1b* (Fig. 5Q−T). LPS/H_2O_2 stimulation significantly enhanced M1 macrophage polarization, which was substantially suppressed by Mag-PEG_{5K}. This suppression was partially reversed by either the PPARγ antagonist GW9662 or the mitochondrial-targeted antioxidant MitoQ, indicating that both PPARγ activation and mitochondrial ROS clearance contribute independently to the polarization regulation. Complete abrogation of Mag-PEG_{5K}'s effect was observed when GW9662 and MitoQ were co-administered, with M1 polarization returning to levels comparable to the model group. Furthermore, MitoQ alone provided only modest suppression of M1 polarization, significantly less pronounced than that achieved by Mag-PEG_{5K}. These results indicate that Mag-PEG_{5K} modulates macrophage polarization through two complementary mechanisms: mitochondrial ROS scavenging and PPARγ activation, which synergistically drive the transition from pro-inflammatory M1 to anti-inflammatory phenotypes, elucidating its neuroprotective mechanism in cerebral I/R injury.

3.5. *Mag-PEG_{5K} pretreatment of macrophages attenuates neuronal damage in a macrophage−neuron co-culture model*

Mag-PEG_{5K} can inhibit M1 polarization of macrophages in the injured microenvironment by scavenging ROS and activating PPARγ. To investigate its impact on the interaction between macrophages and neurons in the cerebral ischemic microenvironment, we established a co-culture system using RAW264.7 macrophages and HT22 neurons with a transwell insert. This system ensures intercellular signal transmission while minimizing nonspecific effects resulting from direct cell contact[44]. HT22 neurons were subjected to oxygen−glucose deprivation/reoxygenation (OGD/R) to simulate cerebral I/R injury (Fig. 6A). Five experimental groups were established: (I) Control, (II) OGD/R (neurons injury only), (III) OGD/R + RAW264.7, (IV) OGD/R + RAW264.7 + Mag-PEG_{5K}, and (V) OGD/R + RAW264.7 + Mag-PEG_{5K} + GW9662.

Compared to the OGD/R group, co-culture with untreated RAW264.7 cells significantly increased the levels of TNF-α and IL-1β in the medium (Fig. 6B and C). It is well-established that macrophage activation occurs swiftly following cerebral I/R injury. Without treatment, a dominant shift towards the pro-inflammatory M1 phenotype is observed, resulting in the robust release of inflammatory mediators, for instance, TNF-α and IL-1β[45]. In contrast, macrophages pretreated with Mag-PEG_{5K} suppressed the production of TNF-α and IL-1β. Notably, GW9662 could abrogate this effect, leading to a respective increase in the levels of these two cytokines compared with the Mag-PEG_{5K}-treated group, which were restored to levels close to those in the untreated macrophage group (Fig. 6B and C). These findings suggest that the primary mechanism by which Mag-PEG_{5K} suppresses macrophage polarization into the pro-inflammatory M1 phenotype is through the activation of the PPARγ pathway.

In the hypoxic microenvironment, TNF-α and IL-1β secreted by M1-type macrophages can trigger neuronal oxidative stress and inflammatory pathways, exacerbating damage[46]. Using DCFH-DA and DHE fluorescent probes, we found that untreated macrophages significantly increased ROS levels in OGD/R-injured HT22 neurons (Fig. 6D−K), consistent with the known role of M1 macrophages in promoting ROS production. Morphologically, HT22 neurons co-cultured with untreated macrophages showed cell body shrinkage and neurite fragmentation (Fig. 6L). Apoptosis assay and live/dead staining confirmed that untreated macrophages significantly increased HT22 cell death (Fig. 6M−O). However, pretreatment of RAW264.7 cells with Mag-PEG_{5K} effectively reduced ROS levels, improved neuronal morphology, and decreased neuronal apoptosis, and GW9662 could antagonize this protective effect. This further confirms the mechanism by which Mag-PEG_{5K} alleviates neuronal oxidative damage and apoptosis by regulating the polarization status of macrophages and reducing the secretion of pro-inflammatory factors.

In conclusion, our results demonstrate that Mag-PEG_{5K} can regulate macrophage polarization by activating the PPARγ pathway, thereby inhibiting pro-inflammatory factor release and attenuating neuronal oxidative damage and apoptosis.

3.6. *Mag-PEG_{5K} reduces cerebral I/R injury*

To investigate the *in vivo* mechanism of action, mice were divided into four groups: sham, tMCAO, magnolol, and Mag-PEG_{5K} group. We investigated the infiltration of Mo/Mϕ in the ischemic hemisphere 24 h after reperfusion in mice. Compared to sham-operated animals, mice in the tMCAO group exhibited a markedly higher number of splenic Mo/Mϕ. This suggests that following cerebral I/R, splenic Mo/Mϕ are rapidly mobilized to the penumbral region. Notably, there was no significant difference in the quantity of brain-infiltrating splenic Mo/Mϕ among the tMCAO, magnolol, and Mag-PEG_{5K} groups (Fig. 7A and B), suggesting that drug treatment does not reduce the infiltration of peripheral Mo/Mϕ into the brain. However, in contrast to the tMCAO model group, both the magnolol and Mag-PEG_{5K} groups displayed a substantial drop in the proportion of $CD86^+$ cells (an M1 phenotype marker) within splenic Mo/Mϕ (Fig. 7C). This indicates that Mag-PEG_{5K} exerts its therapeutic effect on cerebral I/R injury not by reducing infiltration of splenic Mo/Mϕ into brain tissues, but by inhibiting polarization toward the pro-inflammatory M1 phenotype.

To further elucidate the impact of Mag-PEG_{5K} on the local inflammatory microenvironment, we measured pro-inflammatory cytokine levels in ischemic brain tissue by ELISA. Results demonstrated that TNF-α and IL-1β levels were markedly reduced in the Mag-PEG_{5K} group relative to the tMCAO and free magnolol groups (Fig. 7D and E). qPCR analysis further confirmed that Mag-PEG_{5K} treatment markedly downregulated mRNA expression of *Tnf*, *Il1b*, and *Nos2* in the ischemic penumbra (Fig. 7F−H). These results collectively indicate that Mag-PEG_{5K} effectively suppresses post-ischemic inflammatory cascades and ameliorates the local inflammatory microenvironment in injured regions, and exhibits superior anti-inflammatory efficacy compared to free magnolol.

During cerebral I/R injury, excessive ROS are generated, while endogenous antioxidants such as superoxide dismutase (SOD) and

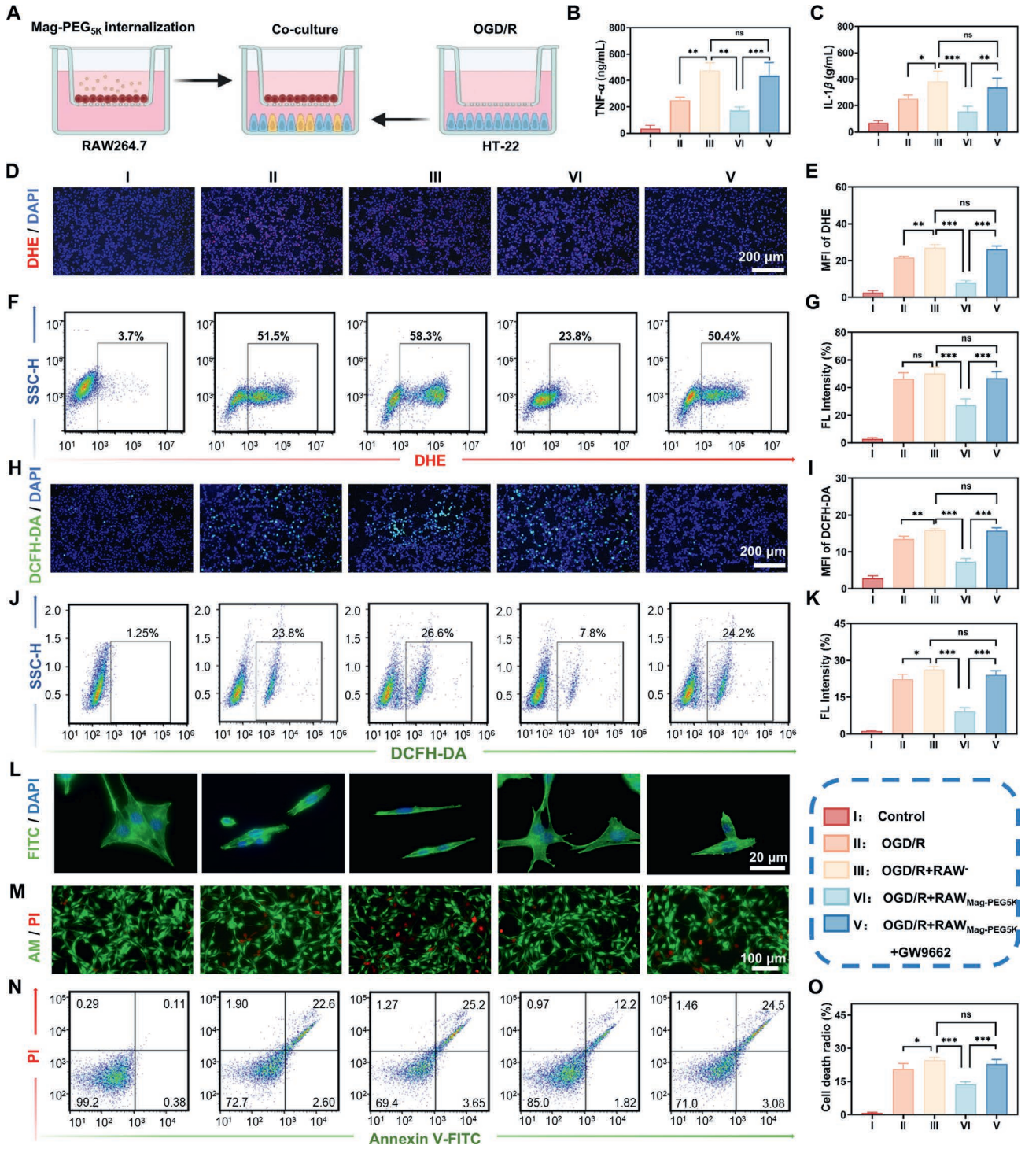

Figure 6 Mag-PEG$_{5K}$ pretreatment of macrophages attenuates neuronal damage in a macrophage−neuron co-culture model. (A) RAW264.7 cells and HT22 cells were co-cultured together in the transwell system. Quantification of inflammatory cytokines (B) TNF-α and (C) IL-1β in the co-culture system ($n = 5$). Fluorescence images and quantitative analysis of (D, E) DHE and (H, I) DCFH-DA staining in HT22 cells, along with flow cytometry plots and statistical results of (F, G) DHE and (J, K) DCFH-DA assays ($n = 5$). Scale bar = 200 μm. Representative fluorescence images of (L) cell morphology and (M) Live-dead staining of HT22 cells. Scale bar = 20 or 100 μm. (N) Representative flow cytometry and (O) statistical analysis of apoptosis in HT22 cells ($n = 5$). Data are presented as mean ± SD. Statistically significant difference: ns (not significant), *$P < 0.05$, **$P < 0.01$, ***$P < 0.001$. One-way ANOVA with Tukey's test was used for statistical analysis.

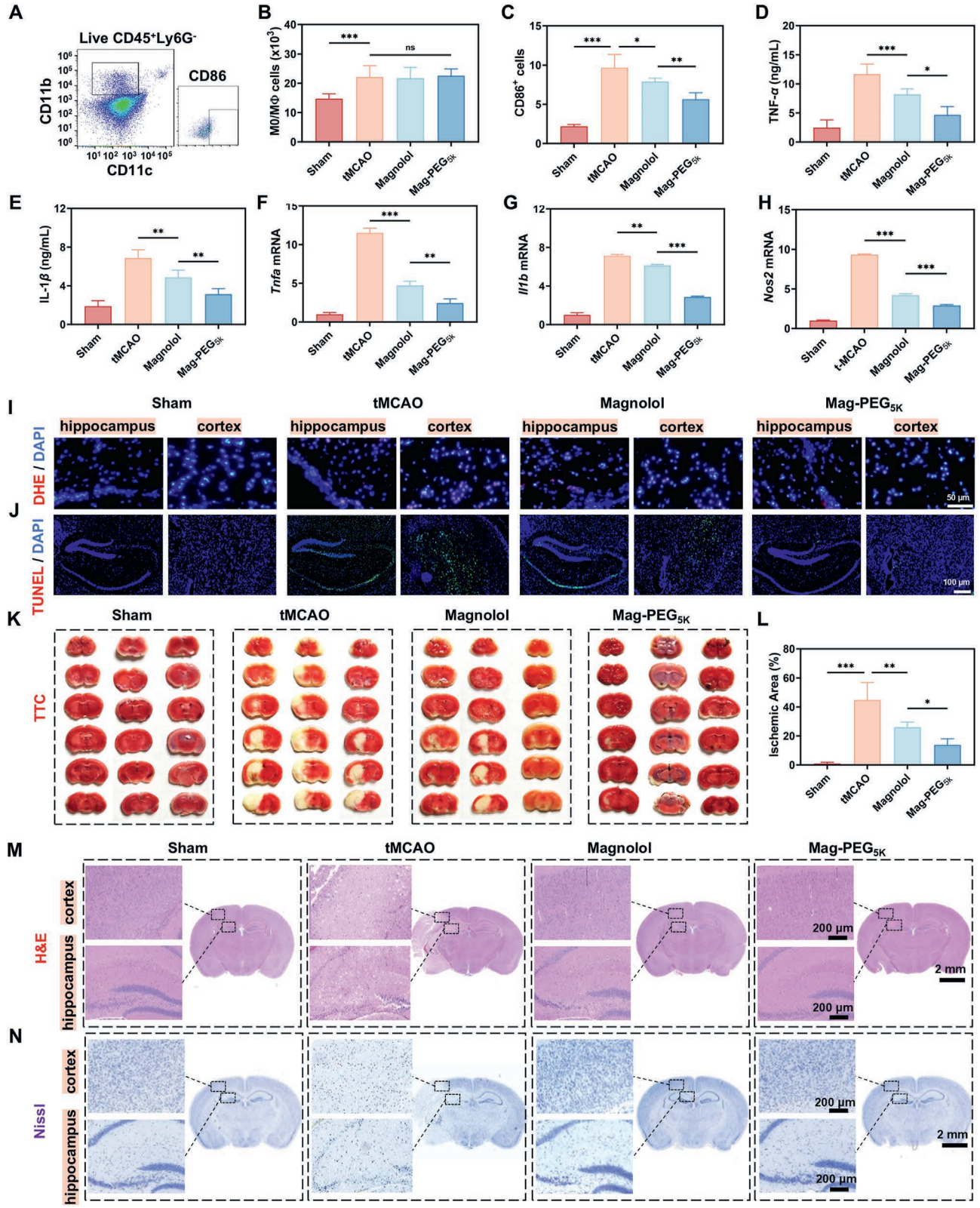

Figure 7 Mag-PEG$_{5K}$ reduces cerebral I/R injury in mice. (A–C) Flow cytometry and quantitative analysis of splenic macrophages (including CD86^{+} subset) in cerebral ischemic regions ($n = 5$). Changes in the levels of the (D) TNF-α and (E) IL-1β in the ischemic penumbra ($n = 3$). Quantitative analysis of (F) *Tnfa*, (G) *Il1b*, and (H) *Nos2* transcripts ($n = 3$). Fluorescent imaging of (I) ROS detection (scale bar = 50 μm) and (J) brain apoptosis analysis (scale bar = 100 μm). (K) Brain specimens and (L) infarct volume quantitative analysis of the brain on Day 3 after cerebral I/R injury ($n = 5$). Representative images of (M) H&E staining and (N) Nissl staining in brain tissue. Scale bar = 200 μm or 2 mm. Data are presented as mean ± SD. Statistically significant difference: ns (not significant), $^{*}P < 0.05$, $^{**}P < 0.01$, $^{***}P < 0.001$. One-way ANOVA with Tukey's test was used for statistical analysis.

glutathione (GSH) are depleted, leading to ROS accumulation[47]. DHE staining revealed significantly elevated ROS levels in the hippocampal and cortical regions of the tMCAO group (Fig. 7I), which were substantially reduced by Mag-PEG_{5K} treatment. This is consistent with its ROS-scavenging effect observed in the *in vitro* experiments described earlier, suggesting that it can improve cerebral ischemia outcomes by alleviating oxidative stress-induced damage.

TUNEL staining assessed neuronal apoptosis[48]. The number of TUNEL-positive cells (indicating apoptosis) increased markedly in the cortex and hippocampus of the tMCAO group but decreased significantly after treatment with magnolol and, especially, Mag-PEG_{5K} (Fig. 7J). TTC staining evaluated cerebral infarct volume post-I/R injury[49]. Three days post-injury, Mag-PEG_{5K} treatment significantly reduced infarct volume compared to the tMCAO and free magnolol groups, demonstrating enhanced neuroprotection at equivalent doses (Fig. 7K and L). Hematoxylin−eosin (H&E) staining showed evident neuronal necrosis with inflammatory infiltration and clear ischemic boundaries in the tMCAO group, while Mag-PEG_{5K} alleviated necrosis and inflammation (Fig. 7M). Nissl staining further validated neuronal damage, showing disorganized neuronal arrangement and dissolved Nissl bodies in the tMCAO group, confirming ischemia-induced injury (Fig. 7N). In contrast, when compared to free magnolol, treatment with Mag-PEG_{5K} resulted in a marked increase in neuronal survival.

In summary, this study demonstrates that spleen-targeted delivery of magnolol *via* Mag-PEG_{5K} offers substantial advantages in treating cerebral I/R injury. Through spleen−brain axis delivery, Mag-PEG_{5K} specifically inhibits the M1 polarization of splenic Mo/Mϕ (rather than reducing their infiltration), thereby effectively suppressing the intracerebral inflammatory cascade, alleviating oxidative stress damage, and reducing neuronal apoptosis. Ultimately, it significantly reduces the pathological damage to neural tissues and decreases cerebral infarct volume. These findings offer a novel theoretical foundation and strategic support for targeting the spleen−brain axis to ameliorate ischemic stroke.

3.7. Mag-PEG_{5K} promotes long-term neurological functional recovery after cerebral I/R injury

Cerebral I/R injury can trigger systemic stress responses, leading to metabolic disorders and subsequent energy negative balance[50]. The process of our behavioral experiment is shown in Fig. 8A. Mice in the tMCAO group lost significantly more body weight and recovered more slowly than other groups, suggesting enhanced persistent catabolism and impaired feeding function in this group. In contrast, the Mag-PEG_{5K} treatment group demonstrated a comparatively minor loss of body weight and a significantly faster recovery rate (Fig. 8B), indicating that Mag-PEG_{5K} can indirectly improve systemic metabolic homeostasis by alleviating brain injury.

The mNSS was used to assess motor, reflex, and balance abilities in mice after cerebral I/R injury[51]. The tMCAO group maintained high mNSS scores over time, indicating persistent moderate-to-severe neurological deficits. Both magnolol and Mag-PEG_{5K} significantly reduced mNSS scores, with Mag-PEG_{5K} showing a greater effect (Fig. 8C). Forelimb use asymmetry was assessed using the cylinder test. The experimental outcomes demonstrated that the asymmetry ratio of mice in the tMCAO group remained at a high level (>0.8) for a long time, which was due to the occurrence of contralateral motor neglect in mice caused by unilateral brain injury. After treatment with Mag-PEG_{5K}, the asymmetry ratio of mice decreased rapidly, showing better efficacy than free magnolol (Fig. 8D). In the adhesive removal test, the tMCAO group took significantly longer to both sense and remove an adhesive patch. The Mag-PEG_{5K} group restored both time parameters to near-sham levels (Fig. 8E and F). Together, these results demonstrate that Mag-PEG_{5K} treatment enhances functional recovery after cerebral I/R injury.

The analysis results of the mouse survival rate during the 28-day observation period are shown in Fig. 8G. All sham-operated mice survived, whereas 75% of tMCAO mice died. Survival rates were 40% and 66% in the magnolol and Mag-PEG_{5K} groups, respectively, indicating that Mag-PEG_{5K} significantly reduced mortality.

Spatial learning and memory in rodents are conventionally assessed using the Morris water maze test. This standardized behavioral assay includes two main phases: the place navigation test (PNT) to evaluate acquisition and the spatial probe test (SPT) to measure retention[52]. In the PNT, tMCAO mice exhibited significantly longer swimming distances than sham-operated controls, indicating impaired spatial learning likely due to hippocampal damage. In contrast, mice treated with Mag-PEG_{5K} showed more direct and efficient trajectories, comparable to the sham group (Fig. 8H). Statistical analysis confirmed that both magnolol and Mag-PEG_{5K} treatments significantly shortened the escape latency and path length to locate the hidden platform compared to the tMCAO group, with Mag-PEG_{5K} showing superior efficacy (Fig. 8J and K). During the SPT (after platform removal), trajectory analysis revealed that tMCAO mice rarely crossed the former platform location, demonstrating profound memory impairment. Treatment with magnolol improved performance, as mice spent more time in the target quadrant and crossed the platform location more frequently (Fig. 8I). Mag-PEG_{5K} treatment yielded further significant improvements, including prolonged time in the target quadrant and a marked increase in platform crossings compared to the tMCAO group (Fig. 8L and M).

Collectively, these results demonstrate that Mag-PEG_{5K} promotes long-term neurological recovery after cerebral I/R injury, as evidenced by improvements in neurobehavioral scores, sensorimotor function, and spatial learning.

3.8. Exploring the biological mechanism of Mag-PEG_{5K} by transcriptomic sequencing

Previous studies have verified that Mag-PEG_{5K} exerts neuroprotective effects by inhibiting M1 polarization of splenic macrophages and reducing the secretion of TNF-α and IL-1β. To explore the downstream mechanism of its action, this study performed RNA sequencing on brain tissues from the Sham group, tMCAO model group, and Mag-PEG_{5K} group.

Principal component analysis (PCA) revealed distinct clustering differences among the three groups (Fig. 9A), with the Mag-PEG_{5K} group exhibiting a gene expression profile highly similar to that of the Sham group but significantly distinct from the tMCAO group. Heatmap and clustering analyses (Fig. 9B) further confirmed these differences.

Volcano plot analysis demonstrated that 1009 genes were significantly upregulated in tMCAO versus sham, and 1437 genes were downregulated in Mag-PEG_{5K} *versus* tMCAO. The intersection yielded 850 core differentially expressed genes (Fig. 9C). KEGG pathway enrichment showed significant enrichment of

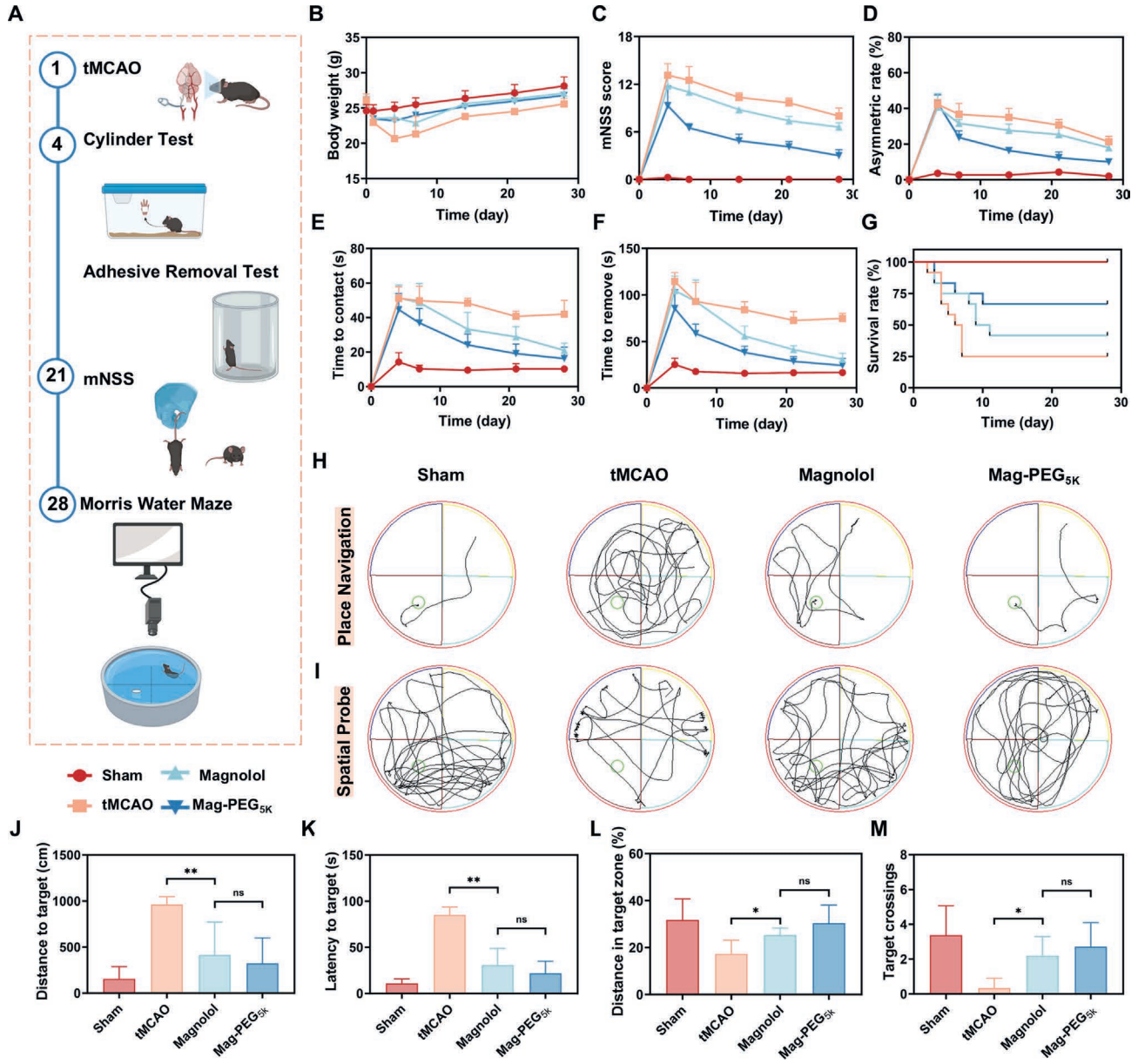

Figure 8 Mag-PEG_{5K} promotes long-term neurological functional recovery after cerebral I/R injury. (A) Mice behavioral tests from Day 1 to Day 28. (B) Body weight statistics and (C) modified Neurological Severity Score of mice. (D) Statistical chart of the cylinder test in mice. (E) Time to contact and (F) time to remove adhesive in forepaws during the adhesive removal test in mice. (G) 28-day survival curve. (H) Representative movement trajectories in the place navigation test across different groups and statistical charts of (J) distance to target and (K) latency to target. (I) Representative movement trajectories in the spatial probe test and statistical charts of (L) distance in target zone percentage and (M) target crossings. ($n = 6-11$, due to mortality during longitudinal observation). Data are presented as mean ± SD. Statistically significant difference: $^{*}P < 0.05$, $^{**}P < 0.01$, $^{***}P < 0.001$. One-way ANOVA with Tukey's test was used for statistical analysis.

these genes in inflammation-related pathways, including MAPK and NF-κB (Fig. 9D). GO analysis further indicated that these genes play central roles in immune responses and inflammatory reactions (Fig. 9E). Furthermore, gene set enrichment analysis (GSEA) confirmed that Mag-PEG_{5K} significantly inhibited chemokine signaling pathways (Fig. 9F) and oxidative stress response pathways (Fig. 9G). These findings collectively imply modulation of immune activation, inflammation, and apoptosis.

To pinpoint key mediators, we intersected target genes related to TNF-α, IL-1β, and cerebral I/R injury from the GeneCard database. A total of 28 core genes were obtained through the Venn diagram intersection, including *MAPK1*, *MAPK8*, *MAPK14*, *NFKB1*, *TLR2*, *TLR4*, and *IRAK1* (Fig. 9H), which are primarily involved in inflammation, immunity, oxidative stress, and neural regulation. KEGG analysis of these genes again revealed significant enrichment in the MAPK and NF-κB pathways (Fig. 9I), highly overlapping with the transcriptomic differentially expressed genes. This convergence indicates that TNF-α and IL-1β act as key initiators, relaying signals *via* a "receptor−adaptor−kinase" cascade. As previously reports[53-55], these cytokines activate the MAPK/NF-κB pathways through specific adaptors (*e.g.*, TNFR/IL-1R), synergize with pathways

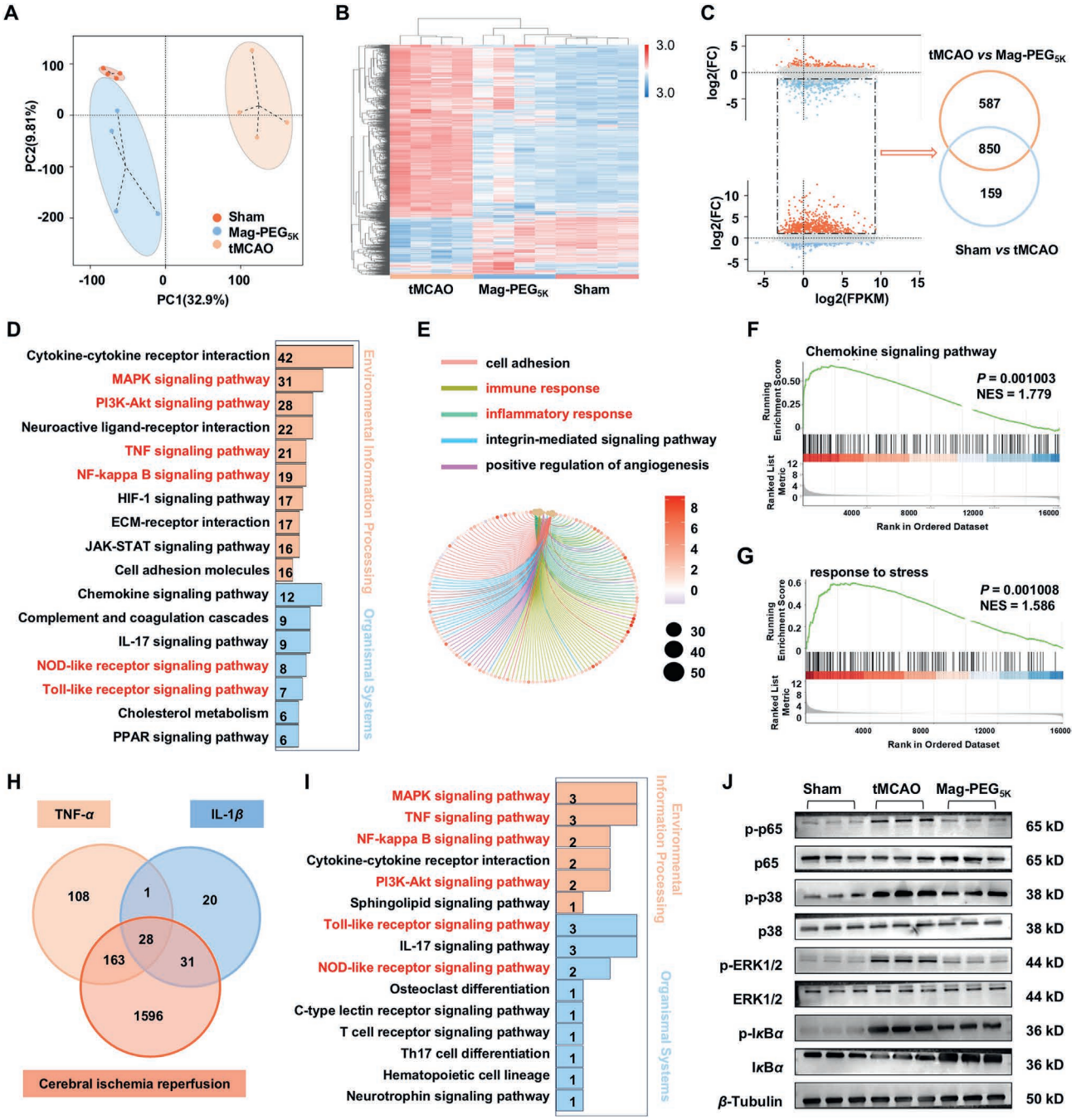

Figure 9 Exploring the biological mechanism of Mag-PEG$_{5K}$ by transcriptomic sequencing. (A) Heatmap plot and (B) PCA results between sham, tMACO, and Mag-PEG$_{5K}$ groups. (C) Volcano plots of genes downregulated in tMCAO *versus* Mag-PEG$_{5K}$, and genes upregulated in Sham *versus* tMCAO, with a Venn diagram comparing these two sets of differentially expressed genes. (D) KEGG pathway and (E) GO enrichment analysis of the intersection genes from (C) Venn diagram. (F, G) Gene set enrichment analysis for chemokine signaling pathway and response to stress in Mag-PEG$_{5K}$ group *vs.* tMACO group. (H) Venn diagrams of the protein action targets of TNF-α, IL-1β, and Cerebral ischemia reperfusion derived from the GeneCard database. (I) KEGG pathway enrichment analysis of the intersection genes from the (H) Venn diagram. (J) Western blot of the protein levels of p-p65, p65, p-p38, p38, *p*-ERK1/2, ERK1/2, *p*-IκBα, and IκBα.

like TLR, and form an integrated network that amplifies the inflammatory cascade and promotes apoptosis. Notably, due to compensatory crosstalk, inhibition of a single pathway may fail due to compensatory activation among other pathways, whereas directly regulating the secretion of cytokines TNF-α and IL-1β through immunosuppression may be a more effective regulatory approach.

To validate whether Mag-PEG$_{5K}$ suppresses these pathways, we performed Western blotting for key mediators. Compared with the sham group, the tMCAO group showed significant upregulation of phosphorylated p65 (p-p65) and IκBα (*p*-IκBα) in the NF-κB pathway, as well as phosphorylated p38 (p-p38) and ERK1/2 (*p*-ERK1/2) in the MAPK pathway, indicating robust pathway activation (Fig. 9J). Mag-PEG$_{5K}$ treatment markedly attenuated these increases,

while total protein levels remained unchanged, confirming that Mag-PEG_{5K} inhibits the activation of both the MAPK and NF-κB pathways, aligning with our transcriptomic findings.

Integrating multi-omics data with experimental validation, we propose that Mag-PEG_{5K} confers neuroprotection through a coordinated cascade: (1) Activating PPARγ and scavenging mitochondrial ROS in splenic macrophages to reduce M1 polarization; (2) Decreasing the secretion of TNF-α and IL-1β in ischemic brain tissue; (3) Disrupting the MAPK/NF-κB amplification cascade to inhibit neuronal oxidative stress; and (4) Suppressing neuronal apoptosis. This cascade regulation, which utilizes spleen−brain axis delivery and blocks inflammatory

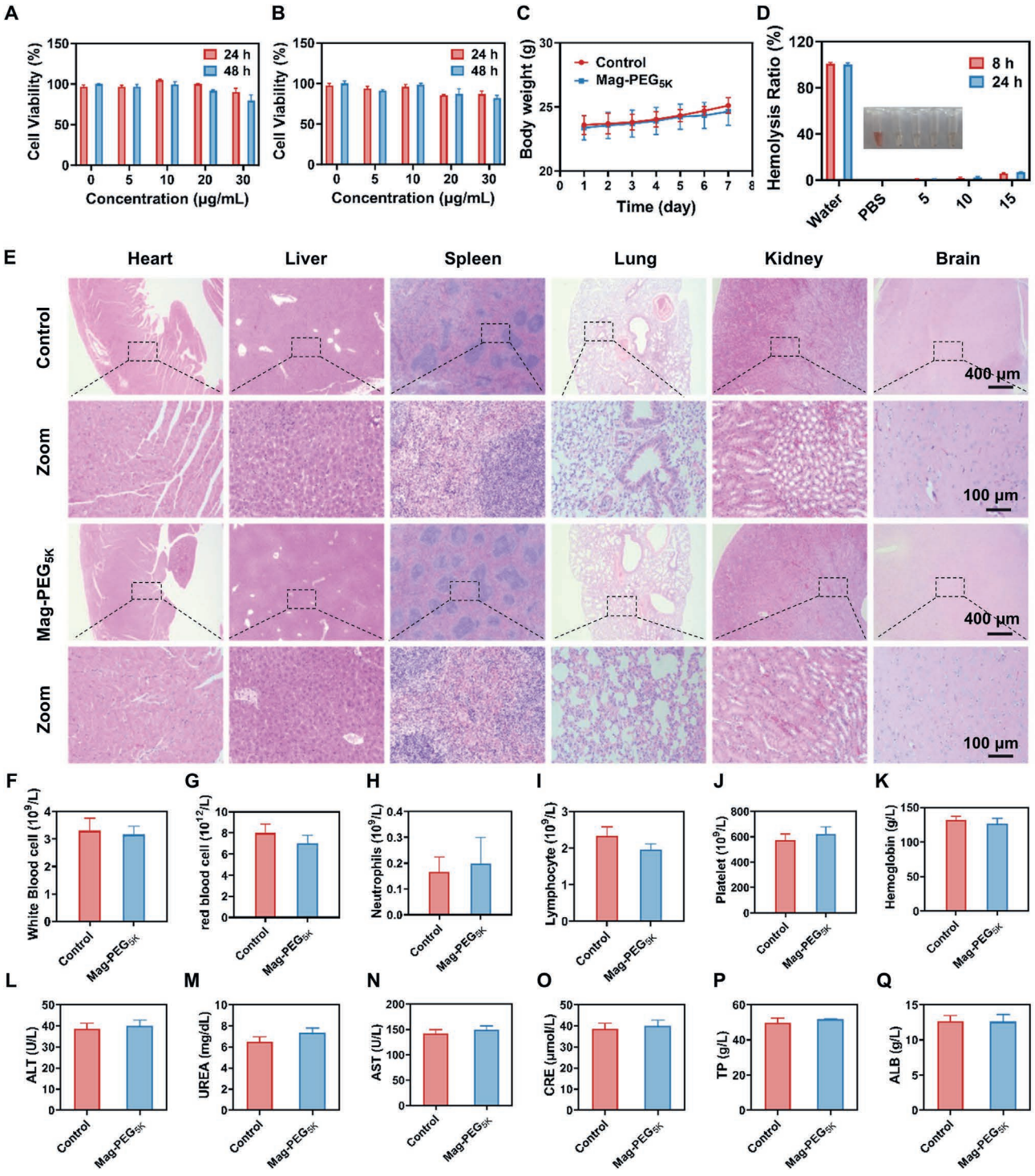

Figure 10 Biocompatibility evaluation of Mag-PEG_{5K}. The viability of (A) RAW264.7 macrophages and (B) splenic Mo/Mϕ following exposure to Mag-PEG_{5K} for 24 and 48 h (n = 3). (C) Body weight variations in mice over 7 days (n = 3). (D) The ratio of hemolysis in the subgroups (n = 3). (E) Major organs harvested on Day 7 underwent histopathological examination with hematoxylin and eosin staining. (F−K) Complete blood count analysis (n = 3). (L−Q) Serum biochemical profiling (n = 3). Data are presented as mean ± SD.

network signals through immune modulation, represents an innovative strategy against cerebral I/R injury**.**

3.9. Biocompatibility evaluation of Mag-PEG$_{5K}$

The biocompatibility of Mag-PEG$_{5K}$ was systematically evaluated at both cellular and animal levels. For *in vitro* studies, RAW264.7 macrophages (Fig. 10A) and splenic Mo/Mϕ cells (Fig. 10B) were treated with Mag-PEG$_{5K}$ (0−30 μg/mL) for 24 or 48 h. After treatment, an MTT assay was performed to determine cell viability. The data demonstrated that cell viability remained above 90% across all tested concentrations and time points, confirming excellent biocompatibility of Mag-PEG$_{5K}$ with cellular systems.

For *in vivo* safety assessment, a mouse tail vein injection model was established, administering 10 mg/kg Mag-PEG$_{5K}$ daily for 7 consecutive days. Body weight changes were monitored daily, and mice were euthanized on Day 7 for organ and blood collection. Results showed no significant differences in body weight between Mag-PEG$_{5K}$-treated and control groups (Fig. 10C). Hemolysis assays (Fig. 10D) revealed no significant hemolytic effects induced by Mag-PEG$_{5K}$. Histopathological analysis, as determined by H&E staining, of heart, liver, spleen, lung, kidney, and brain tissues (Fig. 10E), revealed no treatment-related pathological alterations. Furthermore, hematological parameters (Fig. 10F−K) and serum biochemical indices (Fig. 10L−Q) in Mag-PEG$_{5K}$-treated mice exhibited no statistically significant differences compared to controls. These findings collectively demonstrate that Mag-PEG$_{5K}$ exhibits favorable biosafety profiles both *in vitro* and *in vivo*, providing a solid safety foundation for its application as a drug delivery liposomal system in cerebral I/R injury therapy.

4. Conclusions

In summary, splenic-derived Mo/Mϕ predominantly migrate to the cerebral ischemic region *via* the CCL2/CCR2 chemotaxis axis, which constitutes a critical cellular transport pathway of the spleen−brain axis. The spleen-targeted agent Mag-PEG$_{5K}$ accumulates in the spleen, where splenic Mo/Mϕ internalizes it. Subsequently, these Mo/Mϕ act as "living vehicles", delivering Mag-PEG$_{5K}$ to the ischemic brain region, thereby enhancing its regulatory effect on macrophage polarization. Experimental data confirm that Mag-PEG$_{5K}$ remodels the ischemic microenvironment through a dual mechanism: Mitochondria-targeted delivery significantly amplifies ROS scavenging capacity, and PPARγ pathway activation suppresses M1 macrophage polarization. Collectively, these actions inhibit oxidative stress and inflammatory pathway activation in neural cells, thereby attenuating neuronal apoptosis. Mag-PEG$_{5K}$ effectively promotes histopathological restoration and neurofunctional recovery following cerebral I/R injury. Biosafety assessments confirm its favorable biocompatibility. This study innovatively establishes a spleen−brain axis regulatory therapeutic strategy featuring peripheral immune organ targeting, cellular carrier-mediated drug delivery, and immunomodulatory microenvironment remodeling, providing an endogenous immune system-based pathway for treating cerebral I/R injury. Despite the promising outcomes, the clinical translation of this nanomedicine strategy faces challenges, including ensuring batch-to-batch consistency in large-scale production and evaluating long-term toxicity. Addressing these issues will be crucial for advancing this therapeutic approach from bench to bedside.

Acknowledgments

This work was supported by the National Natural Science Foundation of China (No. 82472127), the Fundamental Research Funds for the Central Universities, China (xtr012025011, xzy022025082), the Key Research and Development Program of Shaanxi Province (2024SF-YBXM-128, 2024JC-YBMS-781, China), and by the International Science and Technology Cooperation and Exchange Program of Shaanxi Province, China (No. 2015 KW-052), the UMCARE Research Fund (UM0125003). We thank Dr. Zijun Ren at the Instrument Analysis Center of Xi'an Jiaotong University for assisting with TEM analysis. The authors are grateful for the convenience provided by all public databases used in this study (Biomarker Cloud and Biorender).

Author contributions

Yane Li: Investigation, Methodology, Data curation, Formal analysis, Writing- original draft. Li Yao: Methodology, Data curation, Formal analysis, Writing- original draft. Jiaxuan Hou: Conceptualization, Methodology, Formal analysis. Xingyu Yuan: Methodology, Formal analysis. Yuanyuan Zhu: Methodology, Formal analysis. Zhichao Deng: Data curation, writing-review&editing. Chenxi Xu: Methodology, Formal analysis. Jinxing Chen: Investigation. Bingyi Chen: Data curation. Jiayan Li: Data curation. Yifan Mei: Data curation. Shuang Liu: Conceptualization. Shaoying Lu: Conceptualization, Resources, Funding acquisition. Mingzhen Zhang: Supervision, Funding acquisition. Hui Cai: Conceptualization, Resources, Writing-review & editing, Funding acquisition, Project administration.

Conflicts of interest

The authors have no conflicts of interest to declare.

Appendix A. Supporting information

Supporting information to this article can be found online at https://doi.org/10.1016/j.apsb.2026.02.012.

References

1. Feske SK. Ischemic stroke. *Am J Med* 2021;**134**:1457−64.
2. Herpich F, Rincon F. Management of acute ischemic stroke. *Crit Care Med* 2020;**48**:1654−63.
3. Paul S, Candelario-Jalil E. Emerging neuroprotective strategies for the treatment of ischemic stroke: an overview of clinical and preclinical studies. *Exp Neurol* 2021;**335**:113518.
4. Mao R, Zong N, Hu Y, Chen Y, Xu Y. Neuronal death mechanisms and therapeutic strategy in ischemic stroke. *Neurosci Bull* 2022;**38**: 1229−47.
5. Ren T, Zhu M, Jiang X, Xu L, Jin H, Zhou Y, et al. Targeting microglial PPARα ameliorates the outcome of ischemic stroke by enhancing interaction with infiltrating peripheral monocytes/macrophages. *Cell Rep* 2025;**44**:115875.
6. DeLong JH, Ohashi SN, O'Connor KC, Sansing LH. Inflammatory responses after ischemic stroke. *Semin Immunopathol* 2022;**44**: 625−48.
7. Dash UC, Bhol NK, Swain SK, Samal RR, Nayak PK, Raina V, et al. Oxidative stress and inflammation in the pathogenesis of neurological disorders: mechanisms and implications. *Acta Pharm Sin B* 2025;**15**: 15−34.

8. Kim E, Yang J, Beltran CD, Cho S. Role of spleen-derived monocytes/macrophages in acute ischemic brain injury. *J Cerebr Blood Flow Metabol* 2014;**34**:1411−9.
9. Leuschner F, Panizzi P, Chico-Calero I, Lee WW, Ueno T, Cortez-Retamozo V, et al. Angiotensin-converting enzyme inhibition prevents the release of monocytes from their splenic reservoir in mice with myocardial infarction. *Circ Res* 2010;**107**:1364−73.
10. Han D, Liu H, Gao Y, Feng J. Targeting brain−spleen crosstalk after stroke: new insights into stroke pathology and treatment. *Curr Neuropharmacol* 2021;**19**:1590−605.
11. Garcia-Bonilla L, Brea D, Benakis C, Lane DA, Murphy M, Moore J, et al. Endogenous protection from ischemic brain injury by preconditioned monocytes. *J Neurosci* 2018;**38**:6722−36.
12. Iadecola C, Anrather J. The immunology of stroke: from mechanisms to translation. *Nat Med* 2011;**17**:796−808.
13. Wang Z, He D, Zeng YY, Zhu L, Yang C, Lu YJ, et al. The spleen may be an important target of stem cell therapy for stroke. *J Neuroinflammation* 2019;**16**:20.
14. Sarrica A, Kirika N, Romeo M, Salmona M, Diomede L. Safety and toxicology of magnolol and honokiol. *Planta Med* 2018;**84**:1151−64.
15. Dong L, Zhou S, Yang X, Chen Q, He Y, Huang W. Magnolol protects against oxidative stress-mediated neural cell damage by modulating mitochondrial dysfunction and PI3K/Akt signaling. *J Mol Neurosci* 2013;**50**:469−81.
16. Yang J, Wei Y, Zhao T, Li X, Zhao X, Ouyang X, et al. Magnolol effectively ameliorates diabetic peripheral neuropathy in mice. *Phytomedicine* 2022;**107**:154434.
17. Hao L, Zhong X, Yu R, Chen J, Li W, Chen Y, et al. Integrating network pharmacology and experimental validation to decipher the anti-inflammatory effects of magnolol on LPS-induced RAW264.7 cells. *Comb Chem High Throughput Screen* 2024;**27**:462−78.
18. Liu X, Chen X, Zhu Y, Wang K, Wang Y. Effect of magnolol on cerebral injury and blood brain barrier dysfunction induced by ischemia−reperfusion *in vivo* and *in vitro*. *Metab Brain Dis* 2017;**32**:1109−18.
19. Li S, Wang Y, Wu M, Younis MH, Olson AP, Barnhart TE, et al. Spleen-targeted glabridin-loaded nanoparticles regulate polarization of monocyte/macrophage (M_o/M_ϕ) for the treatment of cerebral ischemia−reperfusion injury. *Adv Mater* 2022;**34**:e2204976.
20. Sternak M, Glasnović A, Josić P, Romić D, Gajović S. The effects of splenectomy in murine models of ischemic stroke: a systematic review and meta-analysis. *J Neuroinflammation* 2022;**19**:233.
21. Dimitrijevic OB, Stamatovic SM, Keep RF, Andjelkovic AV. Absence of the chemokine receptor CCR2 protects against cerebral ischemia/reperfusion injury in mice. *Stroke* 2007;**38**:1345−53.
22. Bai M, Sun R, Cao B, Feng J, Wang J. Monocyte-related cytokines/chemokines in cerebral ischemic stroke. *CNS Neurosci Ther* 2023;**29**:3693−712.
23. Yang J, Balkaya M, Beltran C, Heo JH, Cho S. Remote postischemic conditioning promotes stroke recovery by shifting circulating monocytes to $CCR2^+$ proinflammatory subset. *J Neurosci* 2019;**39**:7778−89.
24. Xue Z, Shang Y, Yang L, Li T, Yang B. A tailored database combining reference compound-derived metabolite, metabolism platform and chemical characteristic of Chinese herb followed by activity screening: application to magnoliae officinalis cortex. *J Pharm Anal* 2025;**15**:101066.
25. Huang SY, Tai SH, Chang CC, Tu YF, Chang CH, Lee EJ. Magnolol protects against ischemic−reperfusion brain damage following oxygen−glucose deprivation and transient focal cerebral ischemia. *Int J Mol Med* 2018;**41**:2252−62.
26. Zhang J, Chen Z, Huang X, Shi W, Zhang R, Chen M, et al. Insights on the multifunctional activities of magnolol. *BioMed Res Int* 2019;**2019**:1847130.
27. Bai M, Cui N, Liao Y, Guo C, Li L, Yin Y, et al. Astrocytes and microglia-targeted danshensu liposomes enhance the therapeutic effects on cerebral ischemia-reperfusion injury. *J Control Release* 2023;**364**:473−89.
28. Tenchov R, Sasso JM, Zhou QA. Pegylated lipid nanoparticle formulations: immunological safety and efficiency perspective. *Bioconjug Chem* 2023;**34**:941−60.
29. Inglut CT, Sorrin AJ, Kuruppu T, Vig S, Cicalo J, Ahmad H, et al. Immunological and toxicological considerations for the design of liposomes. *Nanomaterials* 2020;**10**:190.
30. Stearne LE, Schiffelers RM, Smouter E, Bakker-Woudenberg IA, Gyssens IC. Biodistribution of long-circulating peg-liposomes in a murine model of established subcutaneous abscesses. *Biochim Biophys Acta* 2002;**1561**:91−7.
31. Oh C, Lee W, Park J, Choi J, Lee S, Li S, et al. Development of spleen targeting H(2)S donor loaded liposome for the effective systemic immunomodulation and treatment of inflammatory bowel disease. *ACS Nano* 2023;**17**:4327−45.
32. Blanco E, Shen H, Ferrari M. Principles of nanoparticle design for overcoming biological barriers to drug delivery. *Nat Biotechnol* 2015;**33**:941−51.
33. Huang Z, Sun K, Luo Z, Zhang J, Zhou H, Yin H, et al. Spleen-targeted delivery systems and strategies for spleen-related diseases. *J Control Release* 2024;**370**:773−97.
34. Wang F, Lou J, Gao X, Zhang L, Sun F, Wang Z, et al. Spleen-targeted nanosystems for immunomodulation. *Nano Today* 2023;**52**:101943.
35. Geng H, Chen L, Tang J, Chen Y, Wang L. The role of CCL2/CCR2 axis in cerebral ischemia−reperfusion injury and treatment: from animal experiments to clinical trials. *Int J Mol Sci* 2022;**23**:3485.
36. Li X, Gao J, Wu C, Wang C, Zhang R, He J, et al. Precise modulation and use of reactive oxygen species for immunotherapy. *Sci Adv* 2024;**10**:eadl0479.
37. Zhang CJ, Li JM, Xu D, Wang DD, Qi MH, Chen F, et al. Surface molecularly engineered mitochondria conduct immunophenotype repolarization of tumor-associated macrophages to potentiate cancer immunotherapy. *Adv Sci (Weinh)* 2024;**11**:e2403044.
38. Van den Bossche J, Baardman J, Otto NA, van der Velden S, Neele AE, van den Berg SM, et al. Mitochondrial dysfunction prevents repolarization of inflammatory macrophages. *Cell Rep* 2016;**17**:684−96.
39. Forrester SJ, Kikuchi DS, Hernandes MS, Xu Q, Griendling KK. Reactive oxygen species in metabolic and inflammatory signaling. *Circ Res* 2018;**122**:877−902.
40. Deng W, Wang X, Niu X, Zhang X, Hou Y, Qin M. Inverse agonists of peroxisome proliferator-activated receptor gamma: advances and prospects in cancer treatment. *J Med Chem* 2025;**68**:9084−100.
41. Fang W, Zhai X, Han D, Xiong X, Wang T, Zeng X, et al. Ccr2-dependent monocytes/macrophages exacerbate acute brain injury but promote functional recovery after ischemic stroke in mice. *Theranostics* 2018;**8**:3530−43.
42. Díaz Acosta CC, Dias AA, Rosa T, Batista-Silva LR, Rosa PS, Toledo-Pinto TG, et al. PGL I expression in live bacteria allows activation of a CD206/PPARγ cross-talk that may contribute to successful *Mycobacterium leprae* colonization of peripheral nerves. *PLoS Pathog* 2018;**14**:e1007151.
43. Hou Y, Moreau F, Chadee K. PPARγ is an E3 ligase that induces the degradation of NFκB/p65. *Nat Commun* 2012;**3**:1300.
44. Shang V, Li J, Little CB, Li JJ. Understanding the effects of mesenchymal stromal cell therapy for treating osteoarthritis using an *in vitro* co-culture model. *Eur Cell Mater* 2023;**45**:143−57.
45. Jian Z, Liu R, Zhu X, Smerin D, Zhong Y, Gu L, et al. The involvement and therapy target of immune cells after ischemic stroke. *Front Immunol* 2019;**10**:2167.
46. Kumari S, Dhapola R, Sharma P, Nagar P, Medhi B, HariKrishnaReddy D. The impact of cytokines in neuroinflammation-mediated stroke. *Cytokine Growth Factor Rev* 2024;**78**:105−19.
47. Shen L, Gan Q, Yang Y, Reis C, Zhang Z, Xu S, et al. Mitophagy in cerebral ischemia and ischemia/reperfusion injury. *Front Aging Neurosci* 2021;**13**:687246.
48. Kyrylkova K, Kyryachenko S, Leid M, Kioussi C. Detection of apoptosis by TUNEL assay. *Methods Mol Biol* 2012;**887**:41−7.

49. Wang Z, Yao M, Jiang L, Wang L, Yang Y, Wang Q, et al. Dexmedetomidine attenuates myocardial ischemia/reperfusion-induced ferroptosis *via* AMPK/GSK-3β/Nrf2 axis. *Biomed Pharmacother* 2022;**154**:113572.
50. Li T, Zhao L, Li Y, Dang M, Lu J, Lu Z, et al. Ppm1k mediates metabolic disorder of branched-chain amino acid and regulates cerebral ischemia−reperfusion injury by activating ferroptosis in neurons. *Cell Death Dis* 2023;**14**:634.
51. Zhao C, Sun L, Zhang Y, Shu X, Hu Y, Chen D, et al. Thymol improves ischemic brain injury by inhibiting microglia-mediated neuroinflammation. *Brain Res Bull* 2024;**215**:111029.
52. Rodríguez Peris L, Scheuber MI, Shan H, Braun M, Schwab ME. Barnes maze test for spatial memory: a new, sensitive scoring system for mouse search strategies. *Behav Brain Res* 2024;**458**:114730.
53. Wang Y, Che M, Xin J, Zheng Z, Li J, Zhang S. The role of IL-1β and TNF-α in intervertebral disc degeneration. *Biomed Pharmacother* 2020;**131**:110660.
54. Zhou W, Li X, Zhou H, Hu Y, Chen Y, Guo D. TNF-α/IL-1β/IL-1α/IL-12 inflammatory cytokine axes coupled with TLR1/TLR3/TLR5/MYD88 immune signaling pathway over-activation contribute to simultaneous carotid and coronary artery and occlusion in elderly patients. *Cytokine* 2025;**185**:156808.
55. Fitzgerald KA, Kagan JC. Toll-like receptors and the control of immunity. *Cell* 2020;**180**:1044−66.